UNIVERSIDADE TÉCNICA DE LISBOA
INSTITUTO SUPERIOR TÉCNICO

The Setup and Engineering Run of the ULTRA experiment

Pedro Jorge dos Santos de Assis

(Licenciado)

Dissertação para obtenção do grau de Mestre em Física

Orientador: Professor Doutor Mário João Martins Pimenta
Co-orientador: Professor Doutor Pedro Miguel Félix Brogueira

Júri:
Presidente: Professor Doutor Mário João Martins Pimenta
Vogais: Professor Doutor António Joaquim Onofre de Abreu Ribeiro Gonçalves
Professor Doutor Pedro Miguel Félix Brogueira
Professor Doutor Luís Humberto Viseu Melo

Dezembro de 2004

Ao Luís

Mudam-se os tempos, mudam-se as vontades,
Muda-se o ser, muda-se a confiança;
Todo o mundo é composto de mudança,
Tomando sempre novas qualidades.

Continuamente vemos novidades,
Diferentes em tudo da esperança;
Do mal ficam as mágoas na lembrança,
E do bem, se algum houve, as saudades.

O tempo cobre o chão de verde manto,
Que já coberto foi de neve fria,
E em mim converte em choro o doce canto.

E, afora este mudar-se cada dia,
Outra mudança faz de mor espanto:
Que não se muda já como soía.

Camões

Resumo

Nesta tese é apresentada a experiência ULTRA que pretende medir o coeficiente de reflexão da luz de Cherenkov gerada por cascatas de raios cósmicos em diversas superfícies, dando-se ênfase ao sistema de aquisição de dados e aos testes realizados.

Pretendia-se desenvolver um sistema distribuído de aquisição de dados com um sistema de sincronismo sem fios. O sistema desenvolvido baseia-se numa placa PCI desenvolvida pelo LIP que permite a aquisição analógica de seis canais com uma precisão de 10 bits e uma frequência de 100 MHz, permitindo também a medição de intervalos de tempo com uma resolução de alguns nanosegundos, com um range dinâmico de mais de 1 segundo. Em conjunto com um sistema GPS que sincroniza o sistema a cada segundo é possível, em cada estação de detecção, adquirir dados e colocar-lhes uma etiqueta temporal, relativa ao UTC, com uma precisão superior a 10 ns.

No último capítulo da tese são apresentados os testes realizados, na região dos Alpes, bem como os seus resultados.

A experiência ULTRA encontra-se, neste momento, pronta para começar as suas tomadas de dados e cumprir assim o seu programa de Física.

Abstract

In this thesis the ULTRA experiment is presented. ULTRA aims to measure the reflection coefficient of the Čerenkov light produce by an Extensive Air shower in several surfaces. The data acquisition system and the engineering runs are described in detail.

It was pretended to develop a distributed DAQ system, synchronized wirelessly. The system developed is based on a PCI board developed by LIP that is capable of acquiring six analog channels with a precision of 10 bits with a 100MHz frequency and measure time intervals with a precision of a few nanoseconds and a dynamic range greater than 1 second. With a synchronism pulse every second from a GPS system it is possible, in every detector station, to acquire events and time-tag each one, relatively to the UTC, with a precision of 10 ns.

In the last chapter of the thesis the ULTRA engineering runs, in the Alps region, and its results are presented.

The ULTRA experiment is, in this moment, ready for physics runs.

Agradecimentos

Começo por agradecer a quem me atura há mais tempo. À Francelina e aos Jorges. Espero que todos me continuem a aturar por muito tempo.

Aos meus amigos da licenciatura, à Susana, ao Jorge, à Tecas, à Inês, à Patrícia, à Catarina, ao David, ao Chambas, ao Bruno, ao Rodrigo, ao TI, ao Moura, ao Tiago, companheiros de aventuras e desventuras.

Ao Mário Pimenta e ao Pedro Brogueira, que me orientaram, por todos os riscos e rabiscos e pela orientação extra-tese.
Ao Luís Melo pelo apoio prestado.

Ao LIP pelas condições proporcionadas para a concretização deste trabalho.
Aos meus colegas do LIP, Patrícia, Catarina, Pedro Abreu, Fernando Barão, por toda a camaradagem.

Ao João Varela, ao José Carlos Silva, ao Miguel Ferreira, ao Siocha e à Paula Bordalo por toda a colaboração prestada.

Ao Jorge e ao João Paulo por me deixarem esventrar os computadores e resolverem os problemas com o software.

À equipa do ULTRA por ter possibilitado a integração do sistema de aquisição desenvolvido.
Ao grupo de Palermo, ao Gino Guggliotta, ao Osvaldo Catalano, ao Livio Scarsi por todo o apoio.

Ao Alan Watson que me indicou o caminho do GPS no inicio.

Ao Bernardo, companheiro de montanha, um agradecimento especial.

Ao Pedro por todo o companheirismo.

Ao Luís, a quem dedico esta tese. Por tudo...

Contents

List of Figures

List of Tables

Chapter 1

Introduction

The ULTRA (Uv Light Transmission and Reflection in the Atmosphere) experiment has been designed, in the context of EUSO [2], to provide quantitative measurements of the reflection/diffusion signal produced by Extensive Air Showers (EAS) impacting on the Earth surface, overcoming the lack of information in this specific field. A conventional scintillator array and UV light detectors ($300 - 400$ nm wavelength range) will operate simultaneously to detect EAS in coincidence with the UV light reflected/diffused from its impact on Earth.

An EAS will be detected in ULTRA by the coincidence of events in several scintillator detectors in the array. The experiment is expected to be carried out at different sites to characterize several reflecting/diffusing surfaces. Depending on the type of surface, the scintillators could be either at fixed positions (ground) or moving (water). In order to allow the foreseen measurements, each element of the array should be equipped with a position determination system. The determination of the shower arrival direction requires precise time synchronization between the array elements.

The synchronization between the several stations of the array and also between the UV light detector and the array is crucial. Traditional acquisition systems tend to drive signal cables from each station to a central acquisition system. In the context of ULTRA, it was investigated the possibility of using a wireless synchronization system based in the Global Positioning System (GPS). The idea to synchronize cosmic ray detectors wirelessly was pioneered in the eighties by the Leeds group at Haverah Park[3].

A low cost, commercially available, GPS is used to synchronize wirelessly a stand-alone custom designed data acquisition board (LIP-PAD). The LIP-PAD board is a PCI based board with two main subsystems: the Analog Acquisition Subsystem (AAS) with six analog acquisition channels and the Time Measuring Subsystem (TMS), with the ability of measuring time intervals with a dynamic range greater than 1s and with a resolution of few nanoseconds. The TMS, the timing part of the LIP-PAD board, uses a 50MHz clock signal derived from a global 100 MHz oscillator and a 100 ps TDC that is driven by Altera

programmable logic. The system was tested in laboratory and used in the engineering runs of ULTRA. Two such runs were performed at Mont-Cenis. A full configuration was installed also for test in the LSPC campus in Grenoble.

The present thesis focus on the development of the ULTRA data acquisition system (chapter 4, 5 and 6) which was my main responsibility in the experiment.

Chapter 2

Extensive Air Showers

Energetic cosmic rays interact with the Earth atmosphere giving birth to Extensive Air Showers (EAS). These air showers are composed by billions of particles (mainly electrons and photons) describing a pencil like shape in space (figure 2.1). At each instant the shower has however the shape of a disk with increasing radius that propagates with a velocity $v \sim c$ (figure 2.2).

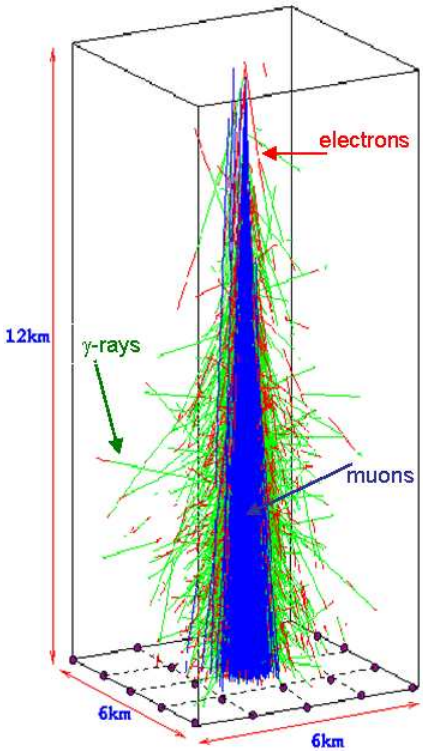

Figure 2.1: Visualization of a simulated EAS.

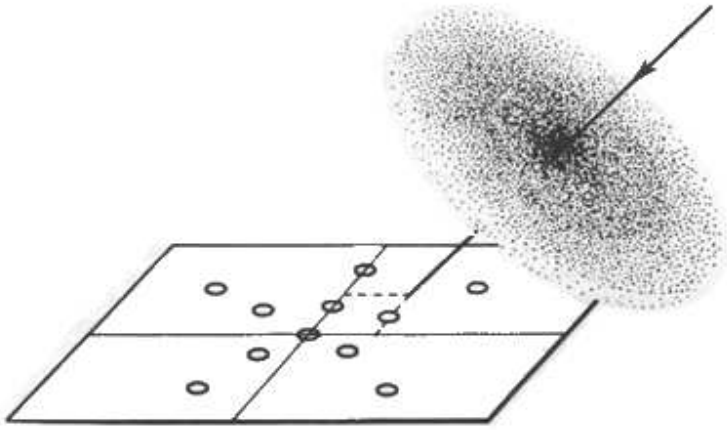

Figure 2.2: The EAS at each instant is seen as a disk of particles with increasing radius that propagate with a velocity $v \sim c$.[1]

2.1 Shower parametrization

The EAS are usually characterized by its longitudinal and transversal profiles. The longitudinal profile (figure 2.3) defines the total number of electrons as a function of the atmospheric depth along the shower axis. The longitudinal profile was parametrized by Greisen [4] as

$$N(t) \sim 0.31 \frac{e^{t\left(1-\frac{3}{2}\ln(s)\right)}}{\sqrt{\beta_0}}$$

with

$$t = \frac{p}{\text{r.l.}}$$

where p is the atmospheric depth and r.l. $= 37.1\ \text{g} \cdot \text{cm}^{-2}$ is the radiation length in air and

$$\beta_0 = \ln\left(\frac{E}{E_c}\right)$$

$$s = \frac{3t}{t + 2\beta_0}$$

with $E_c = 81$ MeV, the electron critical energy. The parameter s is usually called the Shower Age. In the beginning of the shower development this parameter has a value $s = 0$ and in the shower maximum size the parameter takes the value $s = 1$.

The lateral profile (figure 2.4) of the shower gives the particle density in the shower front as a function of the distance to the shower axis and is parametrized by the NKG formula [4, 5]:

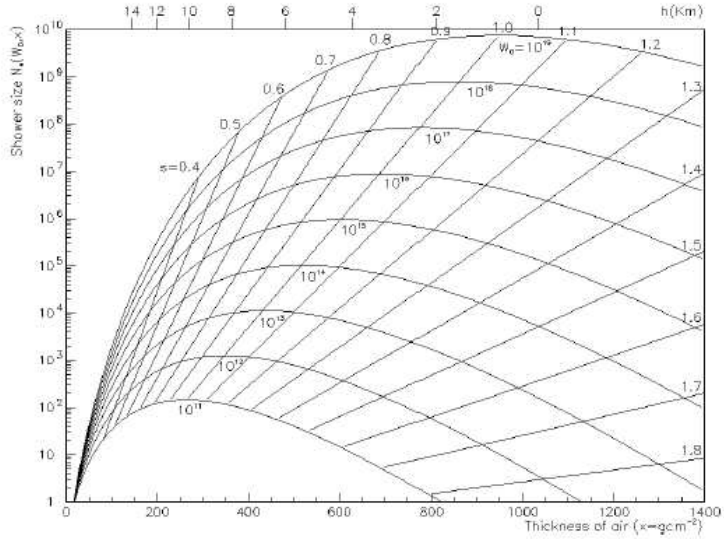

Figure 2.3: Longitudinal development of EAS in air for energies ranging from 10^{11} to 10^{19} eV, as parametrized by the Greisen formula

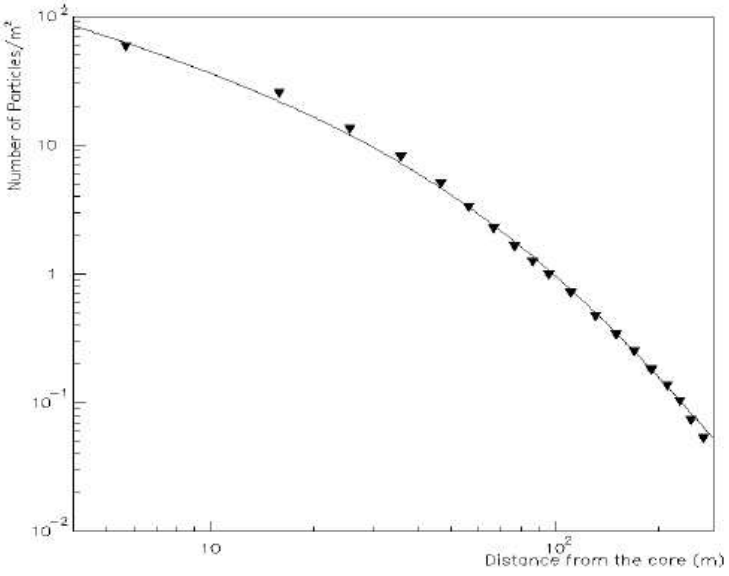

Figure 2.4: Mean Experimental lateral distribution of EAS, measured at 2000 m a.s.l., for showers with $N_e > 10^5$. The line is the best fit to the NKG formula.

$$\rho(r) = c(s)\,\frac{N_e}{r_0^2}\left(\frac{r}{r_0}\right)^{s-2}\left(1+\frac{r}{r_0}\right)^{s-4,5}$$

with

$$c(s) = 0,366 \cdot s^2 \cdot (2,07 - s)^{1,25}$$

where r_o is the Molière radius ($\sim 100\,\mathrm{m}$) and N_e the total number of shower particles.

2.2 Detection techniques

EAS are usually detected by three techniques: sampling the charged particle component using a ground array of particle detectors; collecting the diffused fluorescence light produced by the excitation of N_2 molecules present in the atmosphere by the low energetic electrons; or, finally, collecting the Čerenkov light produced by the relativistic particles of the shower (figure 2.5).

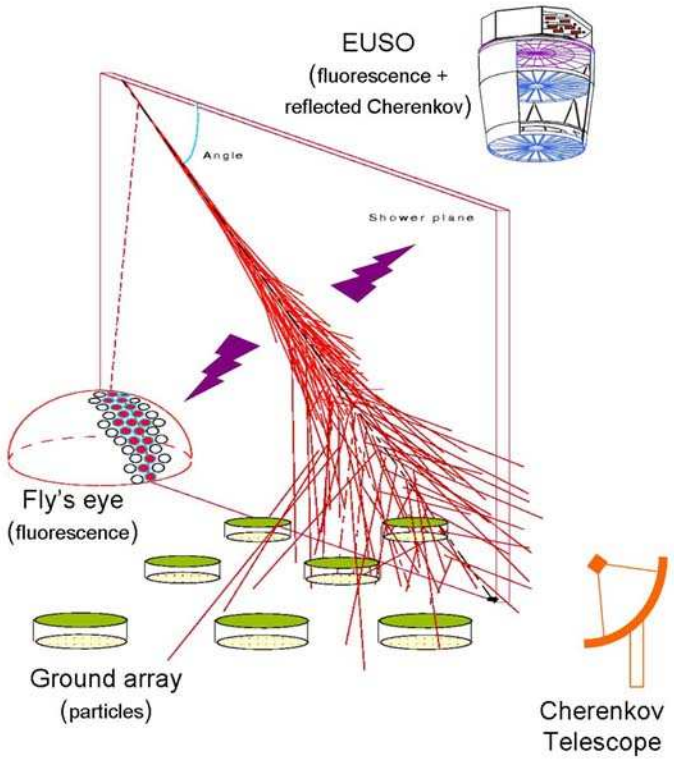

Figure 2.5: detection techniques

The sampling technique relies in the estimation of the particle density in the shower front at different locations. With a scintillator array detector the density

of particles is sampled at each station and then fitted to the shower lateral profile (NKG formula) in order to estimate the shower core and the shower size (N_e). An example of such type of detector is the AGASA (Akeno Giant Air Shower Array) experiment [6] . It uses the sampling technique to study cosmic rays with a primary energy above 10^{17} eV. It consists of a surface array with 111 scintillation detectors and 27 muon detectors spread within a 100 km area, separated by 1 km among them (figure 2.6).

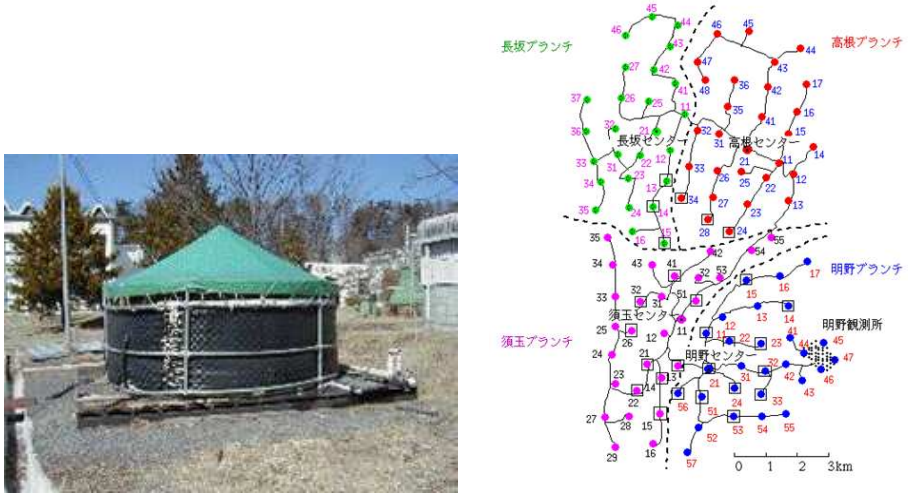

Figure 2.6: The AGASA experiment. Left: One station; right: map of the stations.

As an EAS propagates in the atmosphere , its particles interact with the atmosphere producing light by fluorescence process. Experiments using the fluorescence technique acquire this light to estimate the EAS properties. An example of a detector using the fluorescence technique is the HiRes experiment [7]. Based in the Utah, this experiment is composed by two stations to allow a stereoscopic acquisition of the fluorescence signal from EAS. Each station consists of several detectors to allow a great coverage of the sky. Each detector is, basically, composed by a large spherical mirror and a PMT camera (figure 2.7).

The next important step to increase the statistics of Ultra High Energy Cosmic Rays (UHECR) is the Pierre Auger Observatory (PAO)[8], now in construction in Argentina. PAO is a hybrid experiment having a surface detector, composed by 1600 water tanks in the final configuration and a fluorescence detector composed by 4 stations overseeing the entire surface detector. The observatory will cover an area of about 3000 km^2 and is expected to collect 50 - 100 events per year with a primary energy greater than 10^{20} eV - in one year, more than the present total available statistics. An engineering array has already been built and started operation. Figure 2.8 shows an event from PAO engineering array where it is

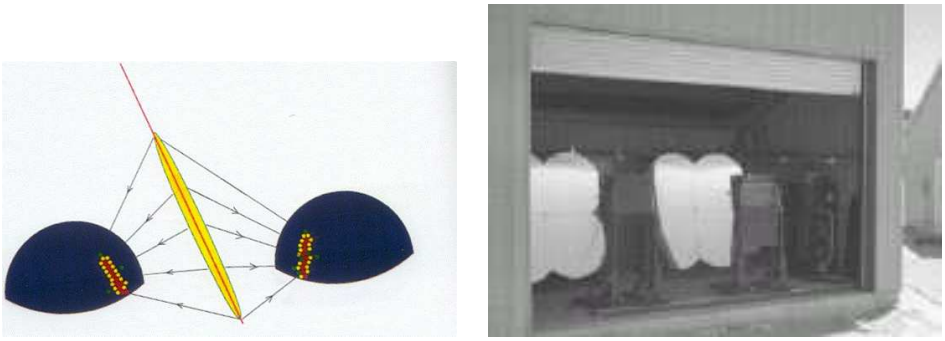

Figure 2.7: The HiRes experiment. Left: sketch of the detection in stereo mode principle. Right: photograph of one fly's eye.

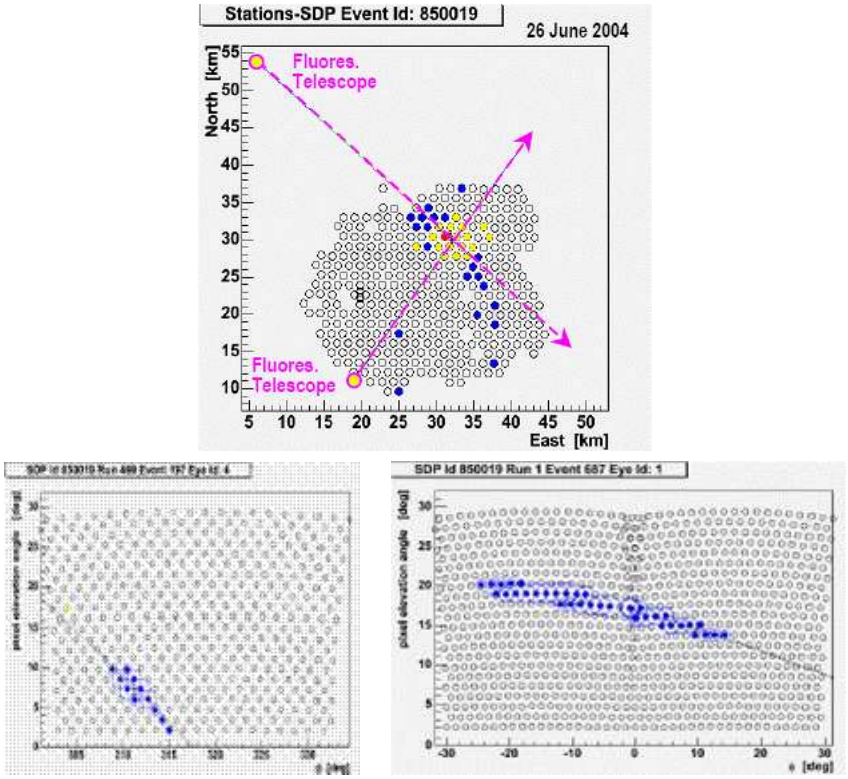

Figure 2.8: An event from PAO. Top: Location of the shower event in the water Čerenkov array; bottom: Signal visualization in the two fluorescence telescopes that acquired the event.

visible the signal in the fluorescence detectors and the water tanks that acquired the event.

To proceed even further a planetary scale detection area is required, only possible with a space-borne approach such as the one to be followed by the Extreme Universe Space Observatory, proposed for 2010. EUSO[2] is a space based fluorescence detector for UHECR detection that will observe an area of $\sim 150000\,\mathrm{km}^2$ and is expected to collect ~ 1000 events with an energy greater than $10^{20}\,\mathrm{eV}$. The EUSO detector consists of an UV telescope to be installed at the International Space Station (ISS) pointing at nadir. Its detection principle (figure 2.9) relies on the detection of the fluorescence light and the reflected Čerenkov light generated by an EAS traversing Earth atmosphere.

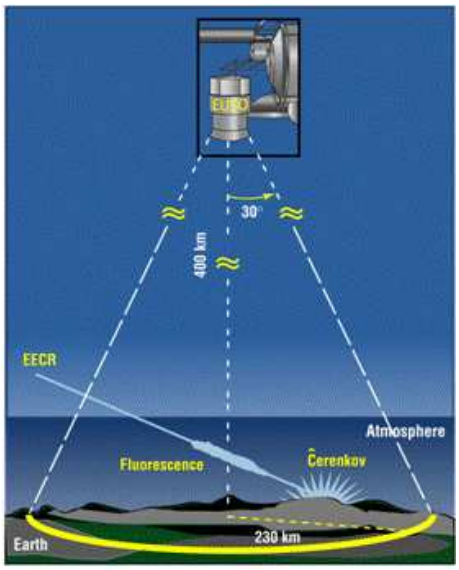

Figure 2.9: Sketch of EUSO detection principle.

The Čerenkov light produced by EAS is also used to detect EAS produced by γ rays in the GeV range. In this case UV telescope with large collecting areas are used to image the Čerenkov light. One example is the MAGIC telescope[9] shown in figure 2.10. This telescope featuring a 17 m diameter mirror is installed at El Roque de los Muchachos observatory in the Canary Islands.

Figure 2.10: The MAGIC telescope. Here with the laser calibration system.

Chapter 3

The ULTRA Experiment

The ULTRA experiment - Ultra violet Light Transmission and Reflection in the Atmosphere is a support experiment for the EUSO mission that aims to provide quantitative measurements of the UV light produced, and reflected in the Earth surface, by an EAS traversing the atmosphere. ULTRA plans to have several runs in order to estimate the signal reflected by several surfaces: rock, grass, snow, sand, water.

The main concept of ULTRA, illustrated in figure 3.1, is to use an UV optical detector, UVscope, to collect the UV light generated by an EAS which is detected with a conventional ground array of scintillators detector, the ETscope.

When the electromagnetic component of a shower is detected by the ETscope relevant parameters such as the arrival direction, the core location and the shower size are estimated. On the other hand the UV light generated by the EAS reaches the ground and is diffusely reflected in every direction. Some of this reflected light reaches the UVscope, where it is detected. The UVscope is placed on a hill pointing downward to a valley where the ETscope is located. The UVscope field of view encloses the area covered by ETscope.

The possibility to measure directly the collimated Čerenkov UV light generated by the EAS before reaching the ground is currently under study with the testing of UV optical modules to be placed in the center of ETscope - Belenos detector.

In the present stage the ULTRA setup, shown in figure 3.2, is designed for ground measurements. In this setup the ETscope is formed by 5 stations disposed in a square with one station in each corner and one in the center of the square. The stations are not autonomous and each station will receive by cable the PMTs high voltage and the PMT signals are driven by cable to a central data acquisition station.

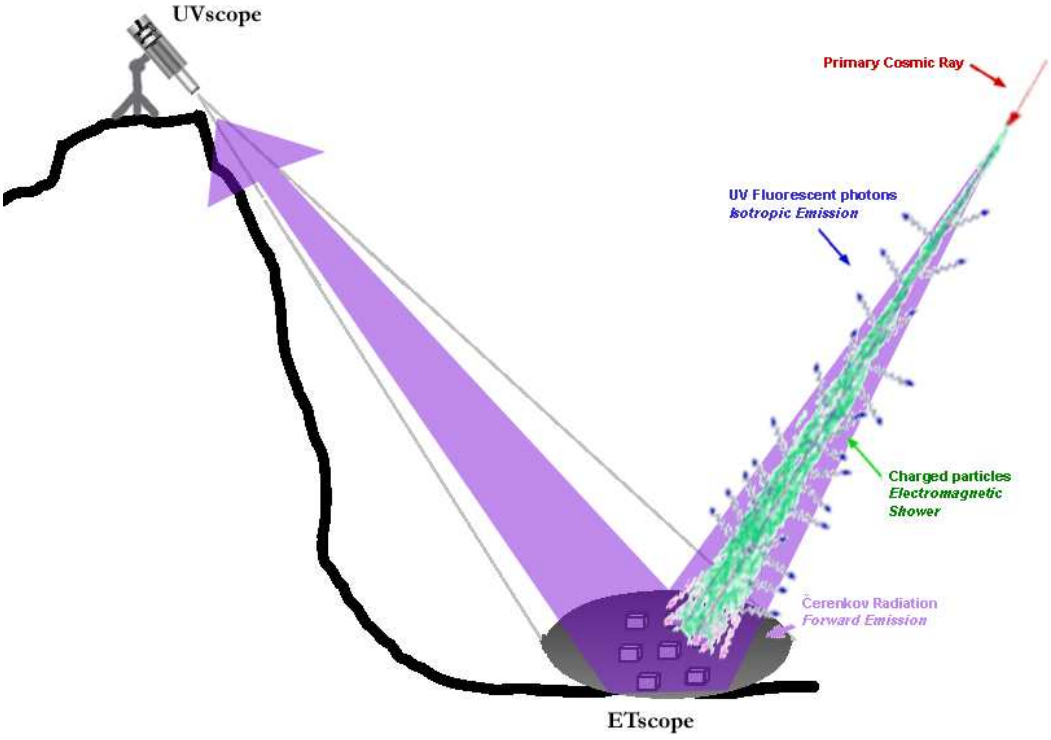

Figure 3.1: The ULTRA operation principle.

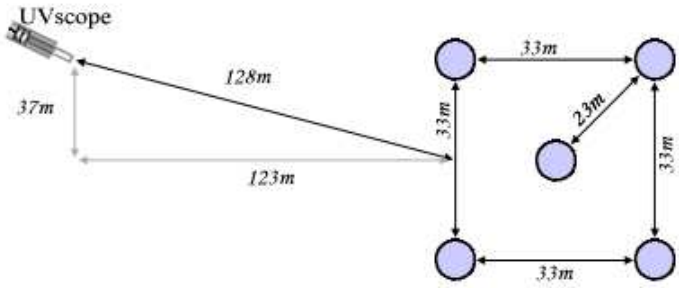

Figure 3.2: View of the ULTRA setup. UVscope is at a higher altitude pointing downward. ETscope is at a flat surface in a valley.

In a later phase the ULTRA setup will be upgraded in order to perform measurements at sea. In this context each station should be autonomous, hence a distributed DAQ system should be used.

3.1 The ETscope detector

The ETscope is a ground array scintillator detector that is used to detect the electromagnetic component of EAS. Each ETscope station estimates the particle density as well as the shower front impact time at the station. Figure 3.3 represents a schematic view of one station which consists of a plastic scintillator, NUCLEAR NE 102A with $80 \times 80\,\mathrm{cm}^2$, 4 cm thick, enclosed in an aluminum pyramidal shaped box which is internally coated with a white diffusing paint. For protection from environmental conditions, each of these boxes is placed inside a PVC container. At the top of the pyramidal box there are two co-located photomultipliers PHILIPS PHOTONICS XP3462B that collect the light generated in the scintillator by a traversing charged particle.

A full simulation of one ETscope station was done by the LIP group [10] using the Geant4 Toolkit package [11]. Figure 3.4 shows the geometry of one station where the scintillator (light blue) and the Pyramidal Box (dark blue) can be seen. The PMTs have been excluded from this representation. The red track represents the traversing charged particle and the green tracks represent the photons generated in the scintillator. For clarity, only 10% of the simulated photons are represented in the figure.

Each PMT, in the configuration presented, receives, at the same time, approximately half of the light signal and thus the coincidence between the two PMT signals eliminates uncorrelated noise. PMT signals are acquired using a custom PCI board - LIP-PAD (see chapter 5 for the description of the LIP-PAD board). To estimate the particle density for an event at one station the energy collected is compared to the deposited energy spectrum for a minimum ionizing particle. The PMT calibration is performed by acquiring PMT signals for minimum ionizing particles.

In shower acquisitions, when a larger dynamic range is needed, one of the PMTs is set to a lower gain. In this configuration the two PMTs will behave differently. The High Gain PMT (hgPMT) is sensitive to minimum ionizing particles (MIPs) while the low gain PMT (lgPMT) is able to acquire high multiplicity events. The gain of the lgPMT is set in such a way that its dynamic range overlaps the range of the hgPMT.

The trigger for shower acquisitions is generated from the hgPMT signals from every station. Two trigger levels are foreseen: the first trigger level is a digital threshold applied independently to each acquisition channel; the second trigger level consists of a programmable coincidence unit. This coincidence unit will generate a trigger whenever, in a time window, a number n of channels of a specified

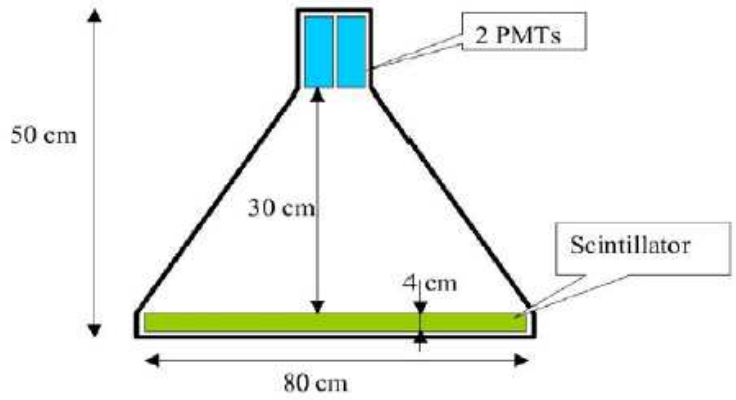

Figure 3.3: Schematic view of one ETscope station

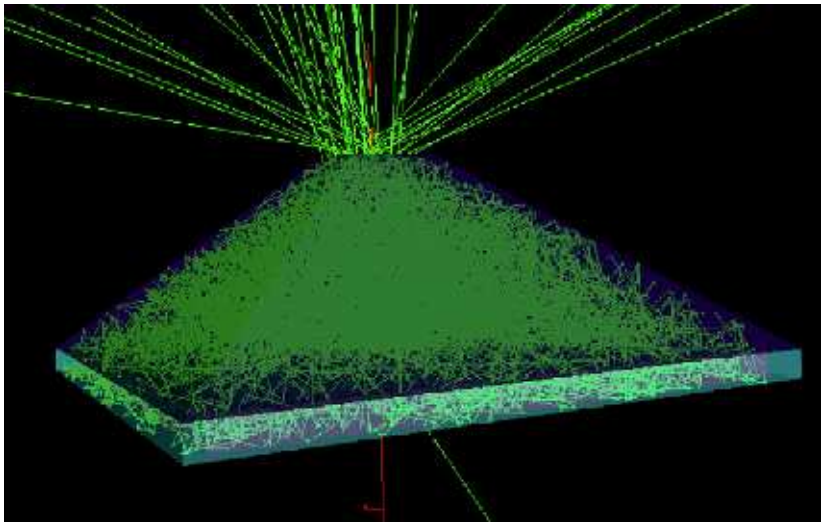

Figure 3.4: Simulation of one ETscope station with GEANT 4

group has generated first level trigger signals. This second level trigger is very flexible since the time window, the required number of channels (n) in coincidence and the set of channels that contribute to the trigger logic are specified by the user.

The calibration of the hgPMT is made acquiring single particle spectra, setting the HV of the two PMTs of each station to the High Gain value and requiring the coincidence between the two signals.

The lgPMT is inter-calibrated with the hgPMT by offline analysis of recorded shower events in the shower operation mode, both by the lgPMT and by the hgPMT, bearing in mind that the light signals that reach each PMT photocathode are similar.

3.2 The UVscope detector

The UVscope is an UV optical detector of the UV light generated by an EAS and diffusely reflected on ground.

The UVscope is a binocular instrument. Each monocle, represented in figure 3.5, consists of a lens and a PMT enclosed in a metal cylinder. The lens used is a Fresnel lens made of UV transmitting acrylic with a diameter of 457 mm and an effective focal length of 441.97 mm at $\lambda = 400$ nm. The PMT has a photocathode with a diameter of 68 mm and is placed on the focal surface defined by the lens. A simulation of the detector has been performed with GEANT4 by the LIP group, see [12]. In Figure 3.6 some images from the simulation output are presented. In the left it is presented the global view of the simulated detector where the envelope (in gray), the Fresnel lens (in red) and the photons tracks (in green) are shown. In the right the detailed visualization of the Fresnel lens (in red) and of the PMT (in blue) is shown. The tracks for perpendicular incident photons are shown in green.

The UVscope acquisition system is also based on the LIP-PAD board and is being developed by the IASF-Palermo Group. It acquires the signal of each photomultiplier and decides the trigger condition. Three trigger modes are foreseen:

- Simple Mode. In this mode the trigger consists of a threshold applied to the output signal of one photomultiplier.
- Coincidence Mode. This trigger mode requires that both PMT have an output signal greater that a threshold at the same time.
- External Mode. In this trigger mode data is acquired whenever an external signal is received. ETscope will generate and send to UVscope a trigger signal when a shower is detected.

If the external trigger mode is used the correlation between UVscope and ETscope data is very simple, since the data is acquired at the same time. If the UVscope

trigger is generated internally it is necessary to synchronize the data acquired. To perform this task it is necessary to time-tag each UVscope event and each ETscope event using a GPS board as described in chapter 4. The data from both detectors is then analyzed offline looking for simultaneous events.

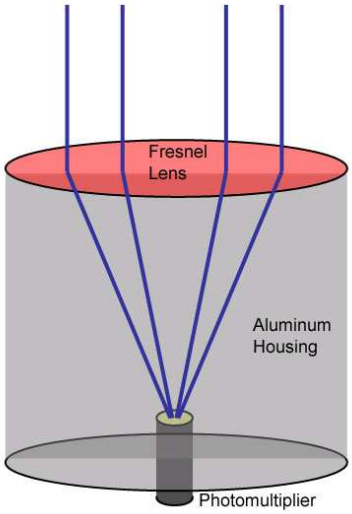

Figure 3.5: Schematic representation of a monocle of the UVscope detector. It consists of a Fresnel lens and a photomultiplier enclosed in an aluminum cylinder.

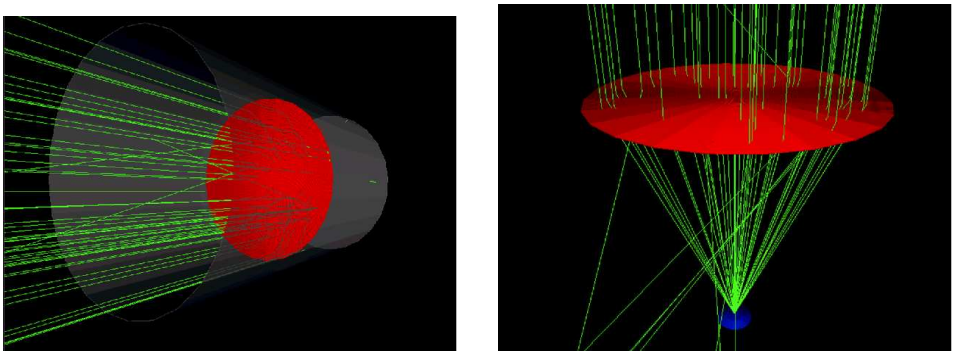

Figure 3.6: UVscope simulation in GEANT4. Left: Global view of the detector; Right: Image of the UVscope Fresnel lens with optical photons tracks represented.

Each monocle will observe the ETscope area. The Fresnel lens allow for the UVscope to have a larger photon collecting area in order to enhance the signal. The PMT will acquire light signals that reach its photocathode. Since the PMT photocathode is placed in the focal surface of the lens and the light source is far away (UVscope is approximately 100 m apart from the ETscope), the field of view

is defined by the lens focal length and by the photocathode area. Considering that the photocathode can be described by a circle then the full field of view of the detector can be estimated by

$$\tan\theta = \frac{d}{fl}$$

where d stands for the photocathode diameter and fl for the Fresnel lens focal length. Considering the instrument geometry the full field of view of the instrument is estimated to be $\sim 9°$.

3.3 ETscope DAQ Requirements

The ULTRA experiment will have two phases. In the first phase several engineering runs will take place. In this phase the stations will not operate autonomously. The signal of each station will be driven by cables to a central DAQ system - Centralized DAQ. In a later phase the stations will operate autonomously and each one will have an independent DAQ - Distributed DAQ.

The Centralized DAQ must:

- Digitize the anode signal of each PMT;
- have at least 10 acquisition channels and have the possibility to upgrade the number of acquisition channels to accommodate a larger number of stations;
- measure the time between events at different stations with a precision better than 10 ns;
- control the HV of each PMT individually;
- be able to define a MIP acquisition trigger performing a coincidence between the two PMT signals of one station;
- be able to define a shower acquisition trigger performing a n-fold coincidence in a programmable time window of PMT signals from different stations;
- interface the UVscope DAQ.

The Distributed DAQ consists of several independent units, one per station. Each unit must:

- digitize the anode signal of the two PMTs of the station;

- time-tag each event using a time reference common to all units and the UVscope, e.g. the UTC time. The UVscope DAQ must also be able to time tag each acquired event with a precision of $\sim 1\,\mu$s;
- define a MIP acquisition trigger performing a coincidence between the two PMT signals of the station;
- be remote controlled;
- transmit data wirelessly;
- provide and control the HV for the two PMTs of its station.

The system must be able to reconstruct shower events from the data acquired by the several units. The data from each station consists of a list of events. Offline, the time and amplitude information of each event at each station will be used to reconstruct shower signals.

In chapter 5 a DAQ system based on a custom PCI acquisition board, developed by LIP, LIP-PAD, is presented. The use of this board, capable of time-tagging events with a precision better than 10 ns, enables the system to be either a centralized DAQ, either a distributed DAQ.

Chapter 4

GPS & time-tagging

The ability to use a low cost, commercially available, GPS to synchronize a wireless, stand-alone, custom designed data acquisition board and detectors is studied. The synchronization signal is the key of a time-tagging system that records each event at each ULTRA station, detecting time differences between any two stations with an accuracy of a few ns.

4.1 GPS system description

GPS satellites act as beacons emitting a synchronization signal at each UTC second. The GPS computes the distance from the satellite to the receiver from: the satellite orbital position; the receiver position taken from an automatic site survey with 10000 points. The GPS receiver acquires the signal, computes the propagation delay and outputs a signal (PPS) synchronized to the UTC seconds.

The errors present in GPS synchronization are mainly due to the inaccurate knowledge of the propagation of the synchronization signal from the satellites to the receivers, namely the propagation in the atmosphere under different atmospheric conditions. The relative accuracy of the PPS pulses between the different data acquisition systems is an important parameter for absolute time-tagging synchronized with differential GPS . Errors can cancel when different receivers have similar signal propagation paths.

In ULTRA, the stations of the ETscope are less than 100m apart and it can be assumed that the signals from a satellite to different stations have the same propagation characteristics. Thus most of the errors can be viewed as systematic errors that cancel when taking time differences from different stations.

4.2 Receiver description

Motorola UT+ ONCORE [13] was selected as a result of a search, based on the absolute accuracy reported, for a low cost, commercially available GPS receiver.

This receiver was also previously chosen by the Auger Collaboration. The manufacturer states an absolute accuracy, of the PPS signal to UTC second, of 40 ns for the UT+ model.

The UT+ transfers by RS232 protocol data such as position, visible satellites and time (year, month, day, hour, minute and second). Each UTC second generates a TTL signal, the PPS, and is simultaneously identified through the serial interface.

The PPS pulse output has a time offset which is different for each PPS and each receiver. This offset is due to the fact that the GPS receiver can only emit the PPS pulse synchronized with the rising edge of an internal oscillator of 10 MHz. Nevertheless, the receiver evaluates the time between its best estimation of the UTC second and the PPS output. Each second, the prediction regarding the following PPS is made available through the RS232 interface - Negative Sawtooth correction (NegSaw). The NegSaw correction varies roughly from -50 to 50 ns. It is therefore imperious to take into account this correction in order to achieve maximum accuracy.

Tests of the GPS receivers were performed to estimate the differential error inherent to the GPS and are described in the next section.

4.3 UT+ performance estimation in differential mode

The data acquisition system of ULTRA was designed to use the GPS in differential mode for improved accuracy. The differential accuracy of the PPS pulses between two co-located UT+ GPS receivers was studied. The measurement scheme used is presented in figure4.1.

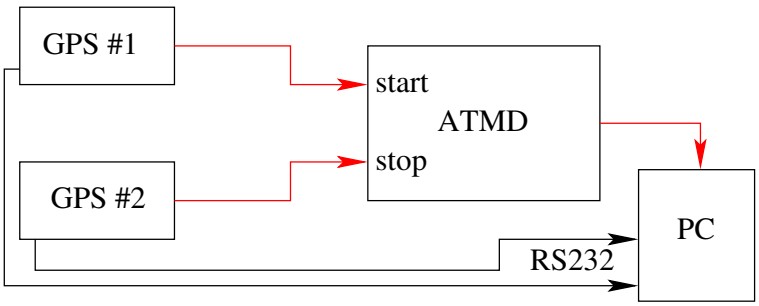

Figure 4.1: Scheme for the measurement of the differential GPS synchronization accuracy.

Two co-located GPS receivers were connected under the same conditions to estimate the different errors inherent to the GPS. Each GPS provided a synchronization pulse each second. The time difference between corresponding PPS

were measured using a Time to Digital Converter TDC - GP1 [14] mounted as a commercial application - ATMD [15] from ACAM. Data from the ATMD and from the GPS, including the NegSaw correction, were recorded in a PC.

Figure 4.2 shows the data from the TDC and the correction to apply. The

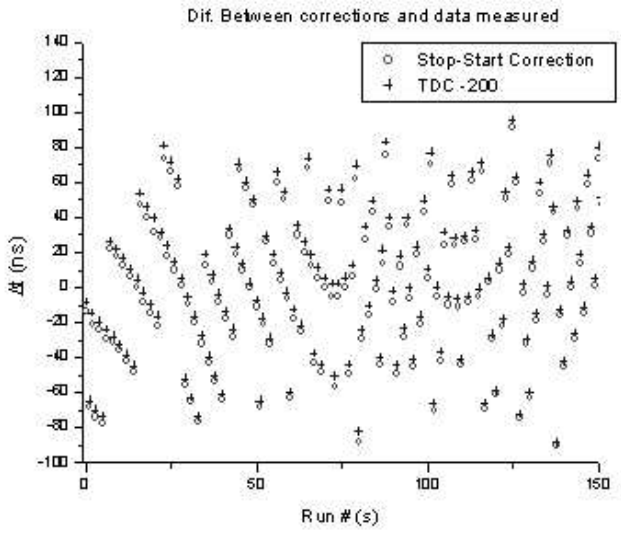

Figure 4.2: Time differences between two co-located GPS obtained from the TDC (+) and differences between the GPSs offset corrections data(∘).

X axis represents the second at which the measurement was made and the Y axis represents the time difference in ns. It is clear that the data has a structure and goes roughly from -100 to 100 ns. The measurements from TDC follow the differences between the GPS's offset correction data. To obtain maximum synchronization precision, time differences will be corrected with the offset correction data.

The corrected data, shown in Figure 4.3, has a lower range of variation and, except for the region around 600 s, where a perturbation has occurred, can be considered to have no important structure. In fact, verifying the serial data collected, it was found that, in this region, the two GPS units were observing a different set of satellites. More, the transitions correspond to the second at which the set of satellites changed for each GPS. This problem can be avoided by pre-programming the set of satellites used by each time-tagging unit.

Figure 4.4 shows the distribution of the time differences calculated from the data collected after the offset correction. The satellites used in this set of data are the same for all the receivers. A Gaussian was fitted to the histogram of the data revealing that the time differences varies around a mean value of 8.3 ns with a dispersion of 2.2 ns. The mean value corresponds to a systematic delay difference

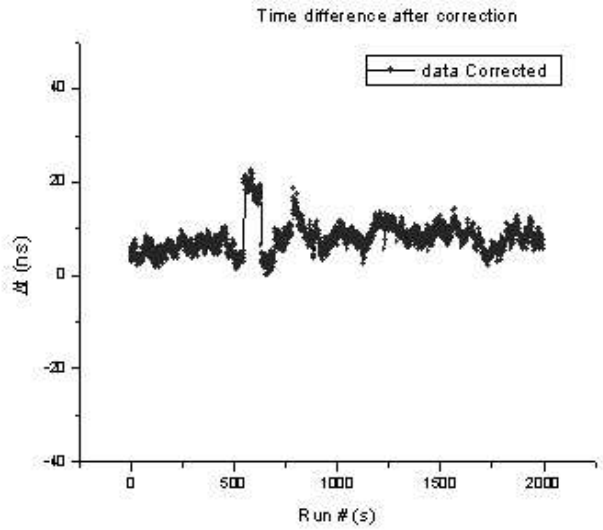

Figure 4.3: Data from fig. 4.2 with the NegSaw correction applied.

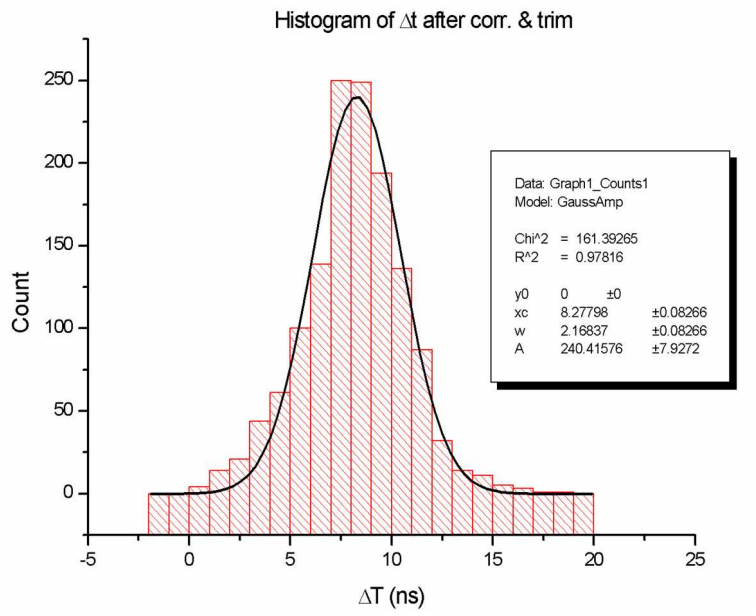

Figure 4.4: Histogram of a set of data collected with the same set of satellites for both GPS receivers.

between the stations and can be eliminated by a proper inter-calibration of each station.

This result was obtained when the conditions for the different receivers are similar. Thus, it is necessary to ensure that the set of satellites used to compute time are the same for all the receivers. This can be done by pre-programming the set of satellites to be used at each time.

4.4 Time-Tagging

The arrival direction of a shower is computed from the differences between the shower front arrival times at the different ETscope stations. In a centralized DAQ system these time differences, which have a dynamical range of a few hundreds ns, are easily measured using a TDC unit. In a distributed DAQ system the arrival time of each event at each station must be registered and then the time differences for the different stations are computed offline.

In the distributed DAQ each station acquires data independently using a coincidence trigger between it's two PMTs. A trigger is generated whenever the signal is above the preset threshold, at both PMT channels.At each station the synchronization signal (PPS) is provided by the GPS receiver at each second. The arrival time of each trigger is then computed (see figure 4.5) measuring the time difference (Δt) between the trigger and the previous PPS, which must be corrected by it's delay (NegSaw) to the nearest UTC second as explained before.

$$T_{\text{trig}} = \text{UTC second} + \text{NegSaw} + \Delta t$$

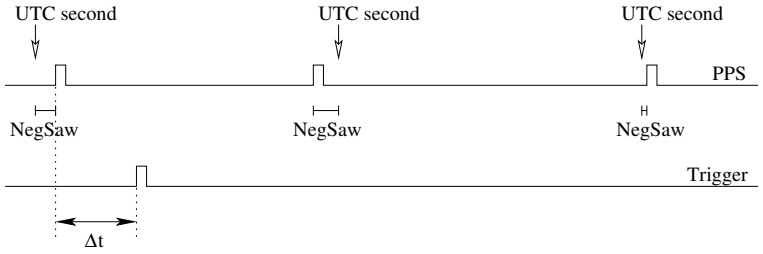

Figure 4.5: Method to Time-tag a trigger. NegSaw is the delay between the PPS and the UTC second. Δt is the time between the trigger and the previous PPS.

To keep the time tagging accuracy in the ns range using the scheme depicted, besides the use of the GPS in differential mode, the computation of the NegSaw correction and the imposition of the same set of satellites for each GPS, the measurement of Δt need to:

- have a resolution of the order of the nanosecond in order to comply with the ULTRA requirement and not to introduce any binning effect, deprecating the overall precision;
- be performed with a dynamic range above one second since the trigger can appear at any time between two consecutive PPS.

To achieve this goal a Time Measuring Subsystem (TMS) was designed and implemented as part of the LIP-PAD board. The TMS developed in the LIP-PAD board consists, basically of a 32 bit, 50 MHz clock (oscillator and counter) and a Time to Digital Converter (TDC). The TDC allows a resolution of 1 ns without a 1 GHz counter, while the use of a clock allows for the desired dynamic range. The measurement method is presented in Chapter 5.2.2 where the TMS is discussed.

Chapter 5

The LIP-PAD board

To fulfill the ULTRA experiment objectives it is desired to have a ground array detector with autonomous stations. Thus each station must have an independent DAQ system with the ability of acquiring/digitizing PMT signals and to time-tag the acquired data. To meet these requirements a custom, PCI based, DAQ board - LIP-PAD board - was developed in cooperation with the Lisbon Cosmic Ray Telescope project (TRC).

Figure 5.1: Photograph of the LIP-PAD board

The LIP-PAD board, shown in figure 5.1, is a PCI based board with two main subsystems: an Analog Acquisition Subsystem (AAS) with six analog, 8 bits, acquisition channels; a Time Measuring Subsystem (TMS), for measuring time intervals with a dynamic range wider than 1s and with a resolution of few nanoseconds. The TMS synchronized by a pulse such as the PPS generated by

the GPS enables the LIP-PAD to time-tag any event better than 10 ns accuracy.

The first version of the LIP-PAD board has already been tested and performs as expected. It has also been successfully tested on field during the engineering runs of ULTRA in Mont-Cenis.

5.1 Block Diagram

The block diagram of the LIP-PAD board is presented in figure 5.2. It´s main components can be grouped in the AAS and in the TMS. The AAS performs the acquisition of the PMT signals and has six analog acquisition channels. Each of these is composed by an analog shaper and a flash ADC. A digital trigger unit and a FIFO memory are also part of the AAS. The TMS is used in time-tagging and measures the time between the synchronization pulse and a trigger signal. The TMS is composed by a TDC and an oscillator. The digital logic associated, both to the AAS and TMS, is implemented on a PLD. In this PLD a PCI interface is implemented. A 100 MHz oscillator is used as a global clock for the AAS (ADCs and PLD). The TMS uses a 50 MHz clock derived from the previous.

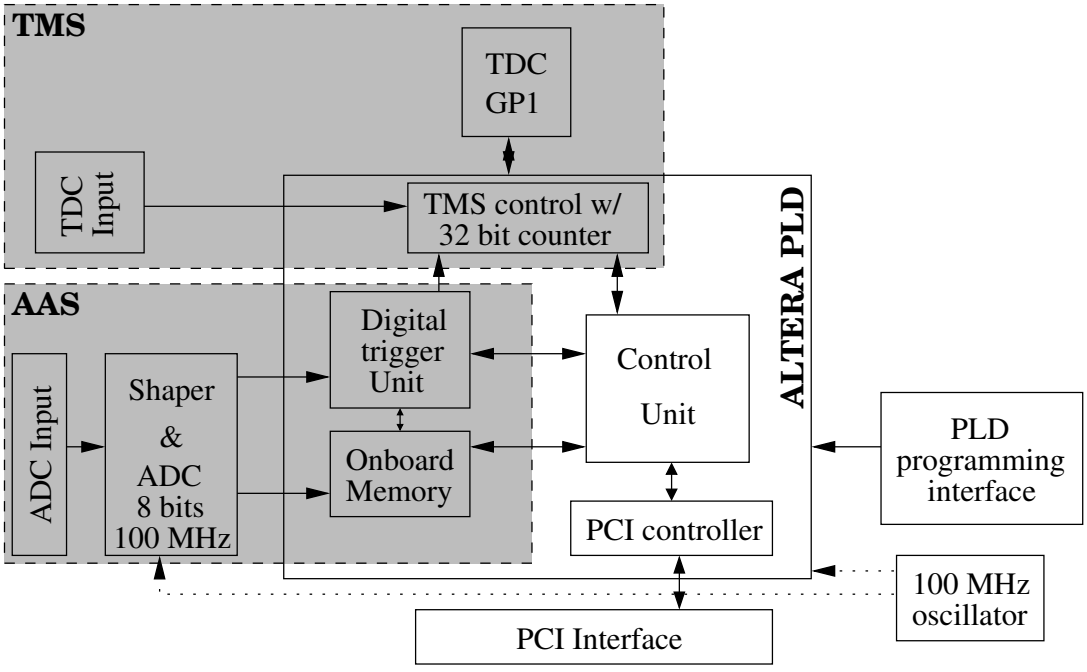

Figure 5.2: Block diagram of the LIP-PAD board

5.2 Functional Description

Within the framework of the ULTRA experiment the LIP-PAD board is used to acquire the PMT signals from each ETscope station in the AAS as well as to time-tag each event for later correlation between each independent station.

5.2.1 Analog Acquisition Subsystem (AAS)

The PMT signals acquired by the AAS are recorded in order to estimate the energy deposited by charged particles crossing each ETscope scintillator. When a charged particle crosses the scintillator looses energy, which is partially emitted in the form of light. This light, generated during a period of few ns, propagates to the PMT where it is converted into an electrical signal. This signal voltage is then sampled at regular intervals of 10 ns and is digitally integrated. The result of the integration is proportional to the amount of light collected, which is, in turn, proportional to the energy deposited in the scintillator.

The AAS consists of six analog acquisition channels of 10 bits. Each channel is composed by an analog shaper and by a flash ADC. Data acquired by the ADC is passed to a Digital Trigger Unit (DTU) and an inboard FIFO memory. The DTU and the FIFO memory are controlled by a Control Unit, which is, in what regards the acquisition process, a five state machine.

For each ADC, the data recorded will consist of a set of PMT samples taken before and after the trigger and it allows to reconstruct the signal and to extract the relevant parameters such as the charge and the time, relative to the trigger, of the event. The amount of data recorded before the trigger is programmable by the user between 0 and the the FIFO maximum depth. Each FIFO in the LIP-PAD was allocated with 256 Bytes of memory, which corresponds, at an acquisition period of 10 ns, to a window of 2.5 μs of acquired data for each trigger.

The work-flow of the Control Unit described in the following paragraphs is shown in figure 5.3. The FIFO behavior in each relevant state highlighted at the Control Unit Diagram is represented in figure 5.4.

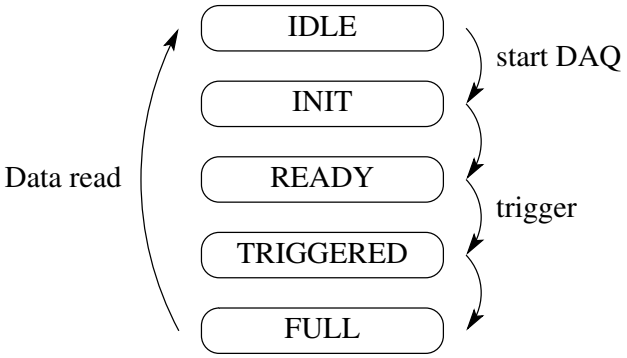

Figure 5.3: Control Unit state diagram

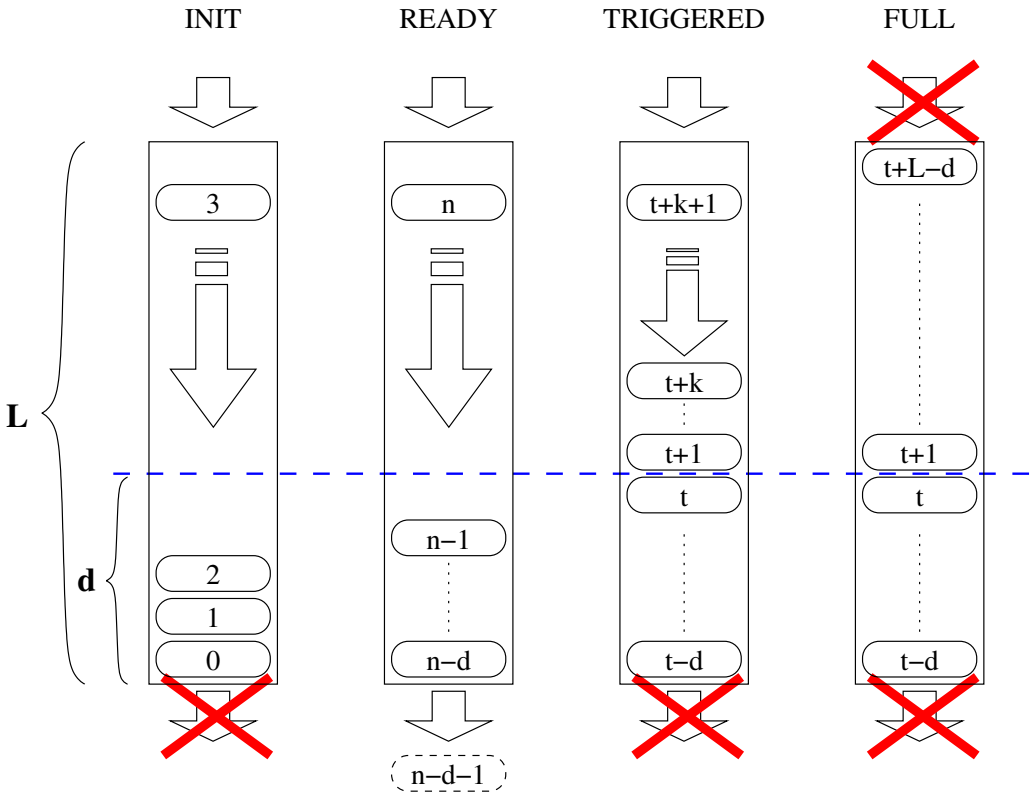

Figure 5.4: FIFO operation modes

- IDLE STATE - In this state the board is idle, waiting for a command to start data acquisition. Data from ADC and trigger signals are ignored. The FIFO memory is offline and empty. The command to start data acquisition causes the state machine to go to the INIT state
- INIT STATE - When a start data acquisition command is given the FIFO

memory has to be prepared before a trigger can be accepted.
In this state the FIFO is partially filled to control the amount of data recorded before the generation of a trigger. In fact one writes a predefined number of words on the FIFO but no read is performed. When this procedure is completed the control unit goes automatically to the next state - READY.

- READY STATE - In this state, at each ADC sample, a write and a read operation is performed on the FIFO. Thus the amount of FIFO occupied remains equal to the predefined. The FIFO behaves then as a memory buffer with a depth, referred in figure 5.4 as "d". When a trigger occurs the state machine goes to the TRIGGERED state.

- TRIGGERED STATE - Data from the ADCs is written in the FIFO and no reading operations are performed. Thus the amount of FIFO occupied grows until the FIFO is completely occupied. This condition is signaled by a FIFO FULL flag and causes the state machine to go, automatically, to the FULL state.

- FULL STATE - The FIFO is full and ADC data is ignored. The board is waiting to be read. When the reading procedure is completed, which is signaled by an empty FIFO flag, the control unit goes to the IDLE state.

Although this acquisition setup is more demanding on the analysis software than a traditional acquisition setup it has the advantage of not performing the integration of the signal online. In fact, there is not a fixed integration window during acquisition and the trigger does not forcibly define the integration region. The signal integration is performed offline. During analysis it is possible to define an offline trigger for each signal and to choose an integration window fitting the region of relevant data. This procedure reduces the background integration, enhancing the Signal to Noise Ratio (SNR).

In a traditional DAQ system, the acquisition of a shower event that generates signals in different stations with different time delays, requires the implementation of a wider integration window which contains all the signals in the different stations. This implementation necessarily increases the background noise.

With the LIP-PAD board the signal is searched offline, in each channel, in a window of 2.5 μs around the trigger, and is integrated only in the region that is relevant. Thus the background integration is reduced and the SNR is enhanced.

5.2.2 Time Measuring Subsystem (TMS)

The Time Measuring Subsystem (TMS) of the LIP-PAD board is used to measure the time between a synchronization pulse and a trigger signal. The TMS must comply with the ns accuracy required having a dynamic range above 1 s since

the GPS synchronization pulses have an average frequency of 1 Hz. It consists, basically of a 32 bit, 50 MHz clock (oscillator and counter) and a Time to Digital Converter (TDC). The use of a TDC allows a resolution of 1 ns without a 1 GHz oscillator while the use of a clock (oscillator + counter) allows for the desired dynamic range above 1 s.

Figure 5.5 represents the measurement scheme of the TMS. The PPS is received in the PLD and it is transmitted to the TDC on channel 1. On the third clock rising edge, after the PPS, a second signal is sent to the TDC on the same channel. The counter value of this rising edge is recorded on a PLD register. The TDC measures the time between the PPS and the clock´s third rising edge after the PPS. When a trigger is received a similar process occurs in the channel 2 of the TDC.

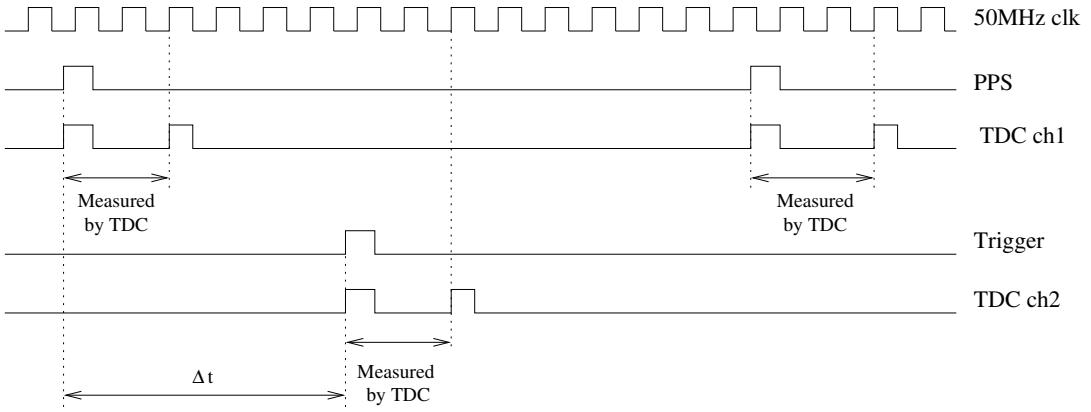

Figure 5.5: TMS measurement scheme.

The time difference (Δt) between the PPS and the Trigger is then a function of the counter values registered for the trigger $\left(\text{count}_{\text{Trigger}}\right)$ and for the PPS $\left(\text{count}_{\text{PPS}}\right)$, the oscillator period $\left(T_{\text{oscillator}}\right)$ and the TDC measurements for the PPS $\left(TDC_{\text{PPS}}\right)$ and for the Trigger $\left(TDC_{\text{Trigger}}\right)$:

$$\begin{aligned}\Delta t &= t_{\text{Trigger}} - t_{\text{PPS}} \\ &= \left(\text{count}_{\text{Trigger}} - \text{count}_{\text{PPS}}\right) \cdot T_{\text{oscillator}} + TDC_{\text{PPS}} - TDC_{\text{Trigger}}\end{aligned}$$

The calibration of the oscillator period can be performed using the same measuring scheme presented above. In fact, for each PPS, the counter value and the TDC data value are recorded. With this data it is possible to calculate the time between consecutive PPS, as measured by TMS.

The manufacturer of the GPS receiver states an absolute accuracy of each PPS to the UTC second of 40 ns. Thus the time between two consecutive PPS is 1 s within 100 ns maximum error (after the NegSaw correction) Taking the

error present in each GPS, the error affecting k s between any k PPS counts is $\varepsilon_{\Delta\text{PPS}} = \sqrt{2} \cdot \varepsilon_{\text{PPS}} = \sqrt{2} \cdot 40\text{ns} \approx 56\text{ns}$

In particular taking two consecutive PPS, the oscillator period is given as:

$$T_{\text{oscillator}} = \frac{1s + \varepsilon_{\Delta\text{PPS}} - TDC_{PPS_{n-1}} + TDC_{PPS_n}}{\text{count}_{PPS_n} - \text{count}_{PPS_{n-1}}}$$

With this scheme the oscillator period can be calibrated with a relative precision of $\sim 10^{-7}$.

The TMS performance was estimated using the experimental setup presented in figure 5.6. It consists of two GPS receivers and two LIP-PAD boards installed in one PC. In this setup the GPS inputs both LIP-PAD boards and cancel their intrinsic errors.

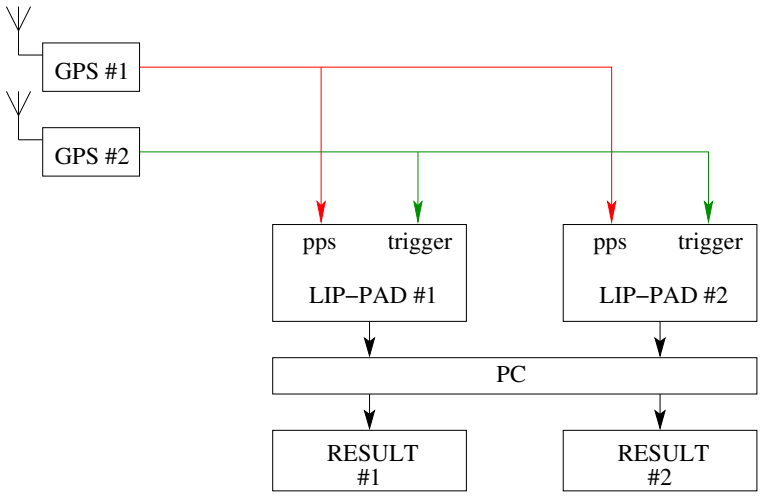

Figure 5.6: Experimental setup for the measurement of TMS performance.

GPS #1 PPS is used as the PPS input both to LIP-PAD #1 and #2. The GPS #2 PPS is delayed internally and is used as the Trigger input to both boards. Each board measures a time between the PPS input and the Trigger input, using the TMS. Both LIP-PADs have, in this scheme, the same PPS input and the same Trigger input. Thus, both TMS should measure, within the errors, the same time. The TMS performance is then estimated by the dispersion of the difference of times measured on the two boards.

The measured data for a programmed delay of 500 ms, half of the TMS dynamic range, is presented in figure 5.7. The X axis represents the number of the sample and the Y axis represents the difference of the times measured by both boards, in ns, after the calibration of the clock oscillator. The distribution of this time difference is presented in figure 5.8.

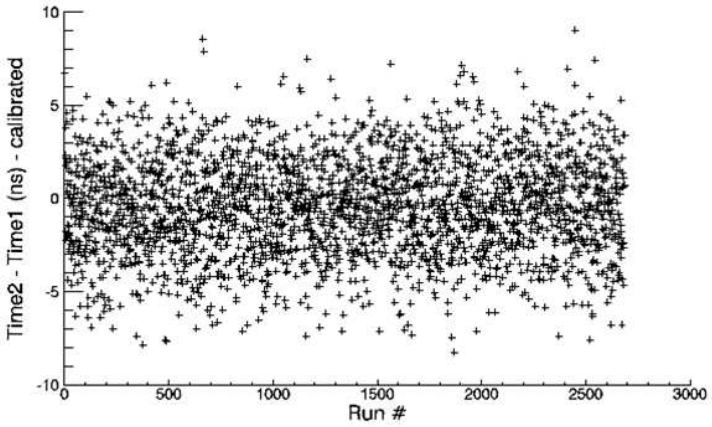

Figure 5.7: Difference between the measured times by each LIP-PAD board versus the acquisition number at an average frequency of 1 Hz

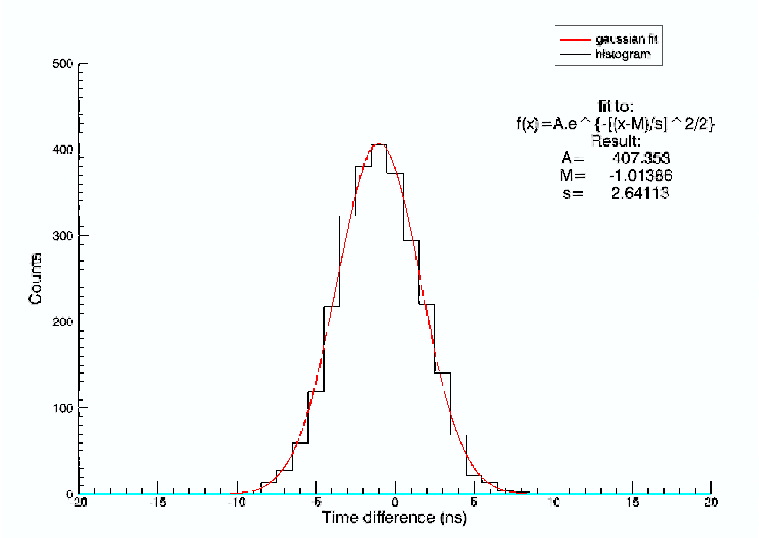

Figure 5.8: Histogram of the data presented in figure 5.7

The mean value is -1.0 ns and the standard deviation is 2.6 ns. The mean value corresponds to a systematic delay difference between boards that can be eliminated by a proper inter-calibration of each board.
The overall performance of the LIP-PAD board to time-tag the event results from the convolution of the error affecting the PPS synchronizing each board with the TMS performance. In particular, the TMS performance in what oscillator period calibration is concerned should be clarified here: the experimental design puts the maximum difference between triggers in each station in the order of 500 ns. Therefore it can be assumed that the error from the calibration of the TMS clock period is of the order of 10^{-3}ns, which is much lower than the PPS pulses synchronization error. If time differences between events approaches 1 s the oscillator period requires the observation of several PPS periods in order to minimize the error.

5.3 Hardware Implementation

The hardware of the LIP-PAD board has three main blocks: analog acquisition channels; time measurement; digital logic.

Each analog acquisition channel is composed by a shaper and a flash ADC. The electronic scheme of the shaper is represented in figure 5.9. The shaper is

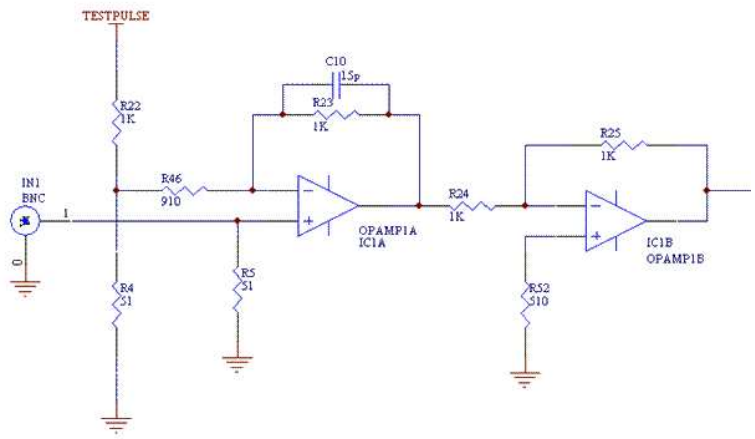

Figure 5.9: Electronic scheme of the analog input shaper

mainly composed by two Operational Amplifiers (OpAmps). The first one has a feedback through an RC filter which controls the shaper parameters. The second OpAmp performs a signal polarity inversion, transforming the negative signal from the PMT in a positive signal, accepted by the ADC. The analog signal is sampled by a flash ADC (ADC08100 from National Semiconductor) which has a

maximum sampling frequency of 100 MSPS, a resolution of 8 bits and a 0 V to 1 V dynamic range.

Time intervals are measured using a clock, composed by a clock signal and a counter, and a TDC. The clock signal is a 50 MHz square wave derived from the global oscillator of 100 MHz which has a precision of 25 ppm. The clock counter is a free running loop counter with a range of 32 bits . The TDC used (TDC-GP1 from ACAM Mess Electronic gmbh) has two measuring channels. Each one has a maximum resolution of 250 ps and is able to measure times from 3 ns to 7.6 μs.

The digital logic is implemented in a PLD (Acex EP1K50QC208-1 from Altera) which has a capacity of 50000 gates and a total RAM bits of 40960.

The LIP-PAD board is implemented as a standard 32 bit, 33 MHz, PCI board. The communication with the PC is performed reading and writing registers in the PCI memory space.

5.4 DAQ software description

Figure 5.10 shows the flow of the acquisition process, where three main blocks are

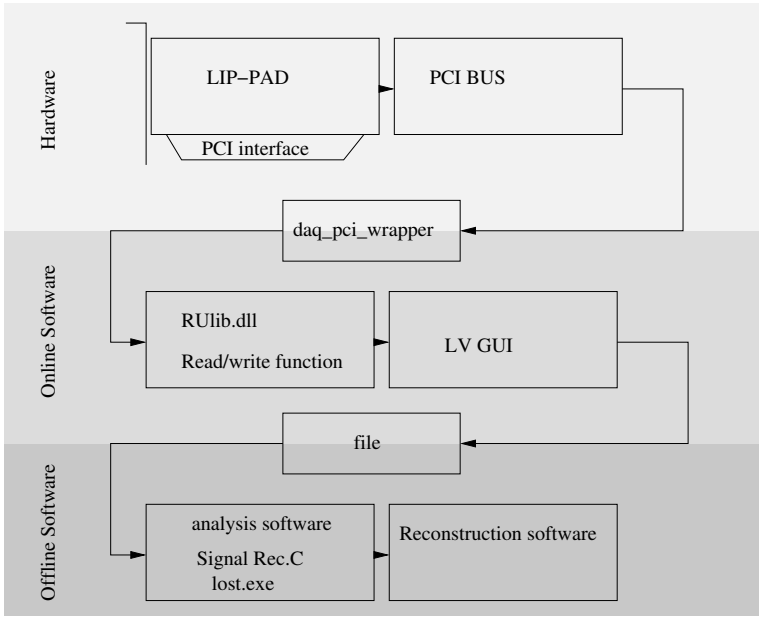

Figure 5.10: Flow of acquisition process

highlighted: hardware - the physical components of the system; Online Software - the software to control and read data during the acquisition; Offline Software - software that performs the data analysis after the acquisition.

Data is acquired by the LIP-PAD and driven through the PCI bus. A module running in the PC microprocessor interface the PCI bus and the RUlib.dll that

runs as online software controlled by a GUI in LV. This GUI saves the data in a file for posterior analysis. The Offline Software estimates from raw data the particle density and time between events at different stations (Signal Rec.C and lost.exe) that will be used to reconstruct the shower direction and size (Reconstruction software).

The DAQ software has evolved from a Linux PCI testing program, developed at CERN (PCIprobe), composed by low level Kernel-space driver to access the PCI bus (daq_pci_wrapper), a C++ library that implements the register Read/Write functions in the User-space (RUlib.dll) , and a Graphical User Interface (GUI), implemented in LABVIEW. The program design allows the user to perform read or write operations to any register in a PCI device.

For the LIP-PAD DAQ this GUI was upgraded to include the various routines that configure and acquire data from the LIP-PAD board in a more automated and user friendly manner. This LV GUI saves the data acquired to a file that is analyzed offline in order to extract the relevant parameters of each signal recorded (signal charge and time). Then a reconstruction software estimates the shower parameters from the signals recorded for several stations.

Figure 5.11 shows the flowchart of the configuration process (left-hand side) and the flowchart of the automatic acquisition routine (right-hand side). In the automatic acquisition mode the user can preset the number of events to be recorded and the data acquired can be saved to a file for a posterior analysis. There is also the possibility to enable or disable the online visualization of the data acquired with the option "plot?".

The main window of the LV GUI is shown in figure 5.12 where some blocks of controls are highlighted.

The LV GUI saves data from an automatic acquisition in a binary file with the structure presented in Table 5.1. For each acquired event a 256 bytes header

...	...
[Event *n-1* Ch. 6]	256 bytes
[Event *n* Header]	256 bytes
[Event *n* Ch. 1]	256 bytes
[Event *n* Ch. 2]	256 bytes
[Event *n* Ch. 3]	256 bytes
[Event *n* Ch. 4]	256 bytes
[Event *n* Ch. 5]	256 bytes
[Event *n* Ch. 6]	256 bytes
[Event *n+1* Header]	256 bytes
...	...

Table 5.1: Structure of the data recorded by LIP-PAD

is saved, followed by six 256 bytes Channel blocks. The header structure is shown

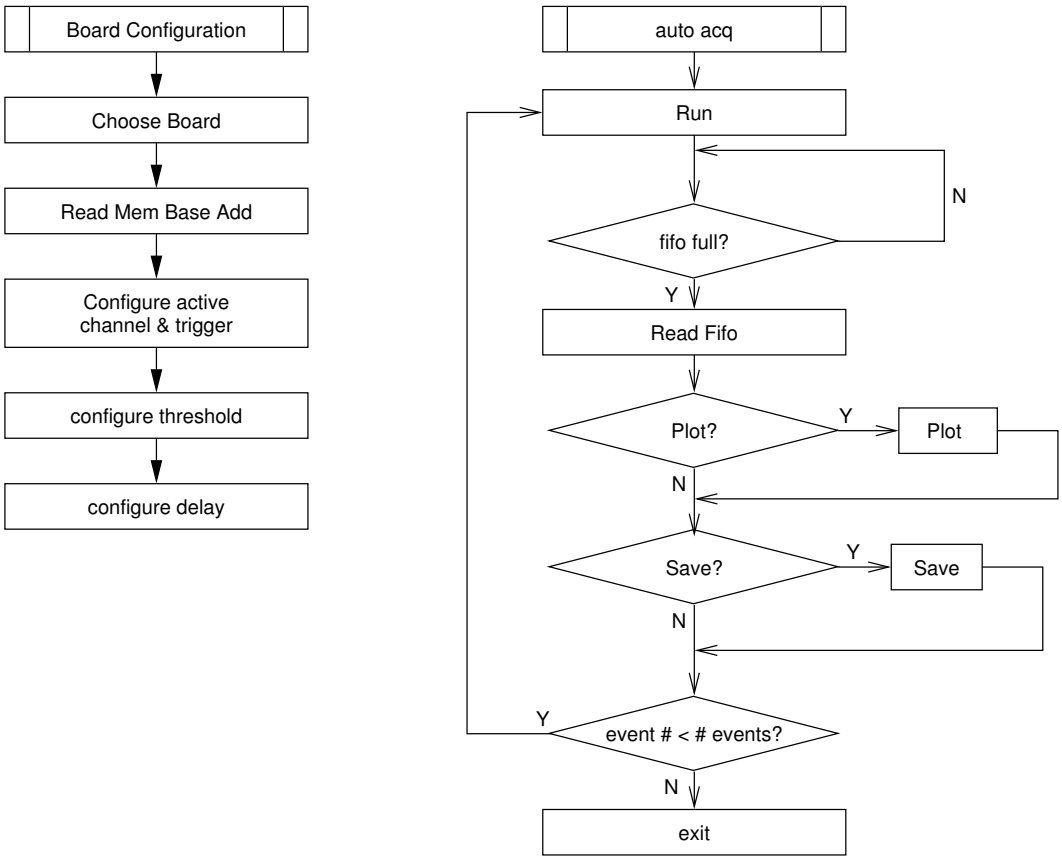

Figure 5.11: Flowchart of the configuration routine (left) and of the automatic acquisition routine (right)

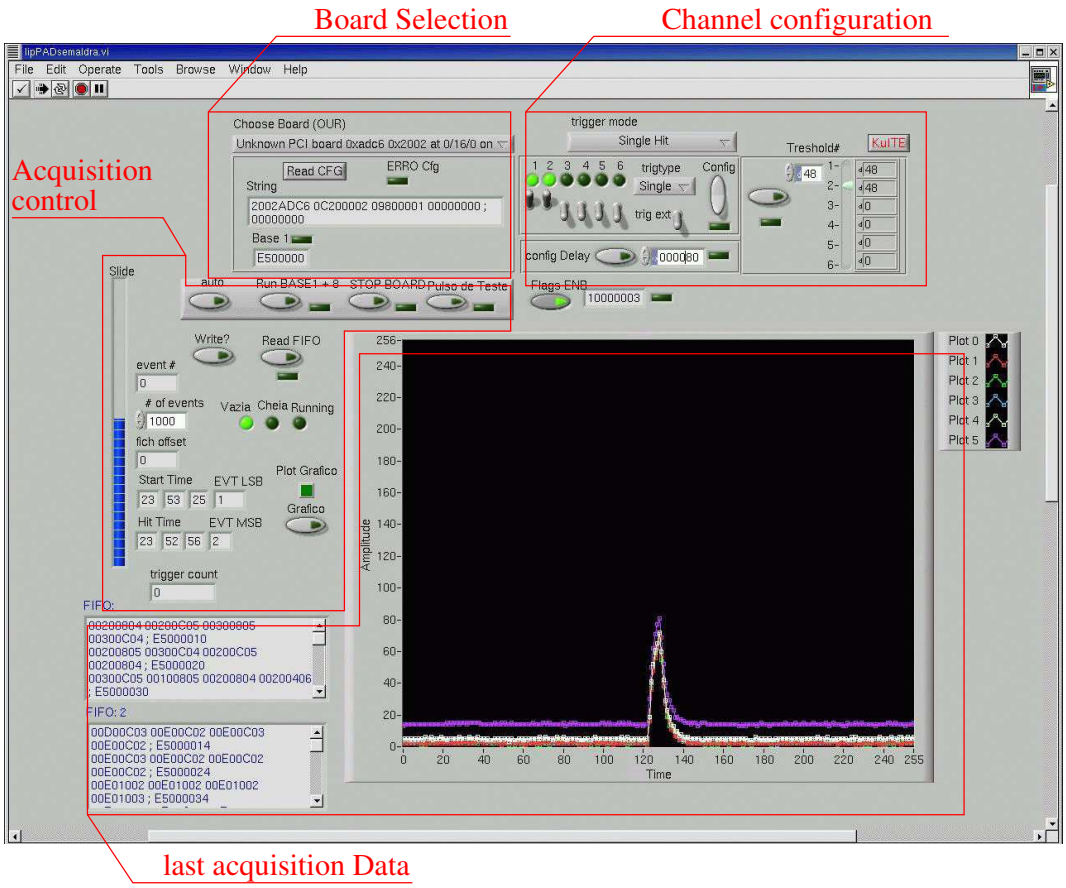

Figure 5.12: Main Analog Acquisition Window

in table 5.2 and, for the moment, contains only the event number , the time at which the acquisition started (Start Time) and the time at which the event was acquired (Trigger Time) . Each channel block has the structure shown in table

Byte	1	2	3	4	5
Data	Event Number			Start Time	
	MSB	LSB	Hour	Minute	Second

Byte	6	7	8	9	10→256
Data	Not Used		Trigger Time		Not Used
		Hour	Minute	Second	

Table 5.2: Header Structure

5.3 and stores the 256 ADC samples that correspond to 2.5 μs of data.

Byte	1	2	...	255	256
Data	V_1	V_2	...	V_{255}	V_{256}

Table 5.3: Channel block structure

Offline, data recorded is pre-analyzed with a C++ program (lost.exe) which main function is to read the file recorded by the LV GUI and to save the raw data in a ROOT tree in order to prepare the data to be analyzed using the ROOT software package. Besides this main function the program performs basic analysis of the data contained in the file and the result is recorded in the ROOT tree. This basic analysis consists in the sum of all data recorded for one channel, the detection of peaks above a threshold and the estimation of the mean time of every peak.

5.5 Signal analysis

The main goal of the signal analysis is to distinguish signals from the background, imposing a digital filter similar to the one used in data acquisition, and then, to extract its relevant parameters. All the analysis software was developed using C++ and ROOT. The extraction of the signal parameters is done fitting the selected events to the following empirical parametrization [16]:

$$V(t) = A \cdot e^{-\frac{1}{2\omega^2}\cdot \log^2\left(\frac{t-t_0}{\Delta}\right)}$$

where the parameters A, w, t_0 and Δ are free parameters. This parametrization, basically describes a fast charge and a slower discharge of a capacitor. Figure

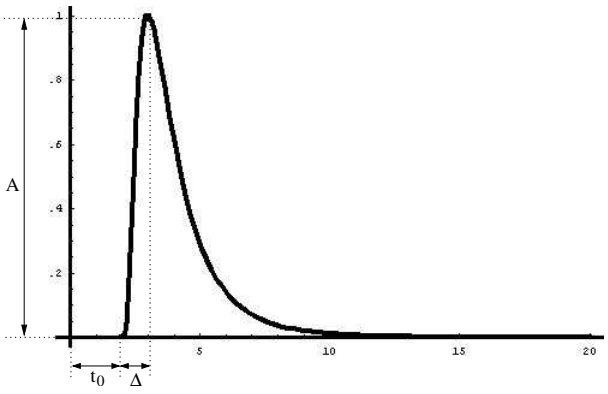

Figure 5.13: Sample curve obtained from the parametrization of the signal shape.

5.13 shows a sample curve obtained with $A = 1$, $w = 0.7$, $t_0 = 2$ and $\Delta = 1$. The parameter A controls the value at the maximum, t_0 is the time at which the signal starts, Δ is the time elapsed between the beginning of the signal and the maximum and ω controls the length of the signal in an non-linear way.

The charge of the signal is estimated by integrating the signal voltage:

$$Q \propto \int V(t) = a \cdot \Delta \cdot e^{0.5 \cdot \omega^2} \cdot \sqrt{2\pi} \cdot \omega$$

The analysis of signals that spread over a wide range of amplitude poses some problems in the determination of the time of the signal[17]. Figure 5.14 shows the

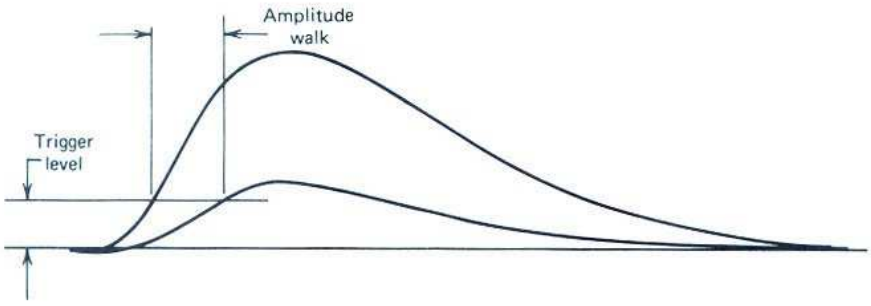

Figure 5.14: The amplitude walk effect. Two signals with the same shape and same starting time are shown. The use of fixed amplitude levels result in different timing.

variation in the time determination of signals with amplitude variation when a fixed amplitude level is used to estimate the signal time. This variation is usually referred to as "amplitude walk" and it is suppressed using a constant fraction

timing, i.e., to take the time at which the amplitude crosses a constant fraction of the maximum amplitude. It is empirically found that the time jitter is minimal when the fraction is set in the region of $10\% - 20\%$. It was chosen to set this value at 20%. Thus, the time of each reconstructed signal is estimated as:

$$t_{20\%} = t_0 + \Delta \cdot e^{-\left(2\omega^2 \cdot \log(5)\right)^{\frac{1}{2}}}$$

Figure 5.15 represents the raw data for a MIP signal acquired with the LIP-PAD. In Figure 5.16 the curve with the parameters from the fit is superimposed with the data

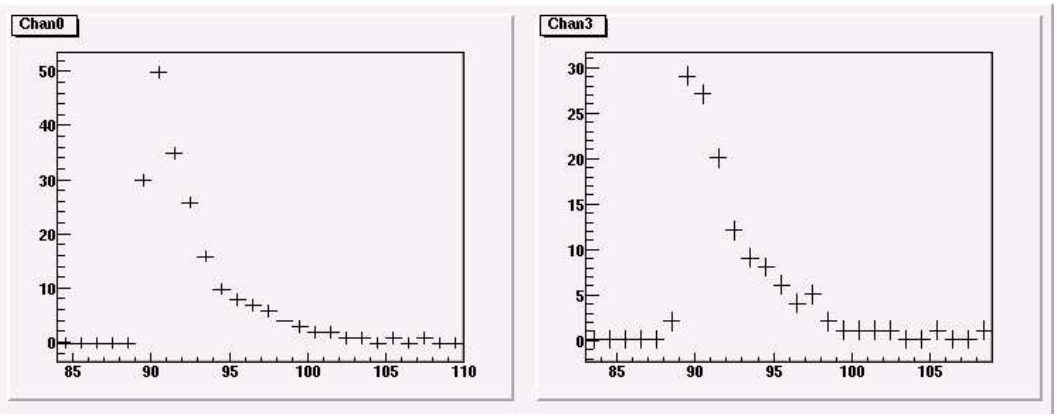

Figure 5.15: Signal Sample

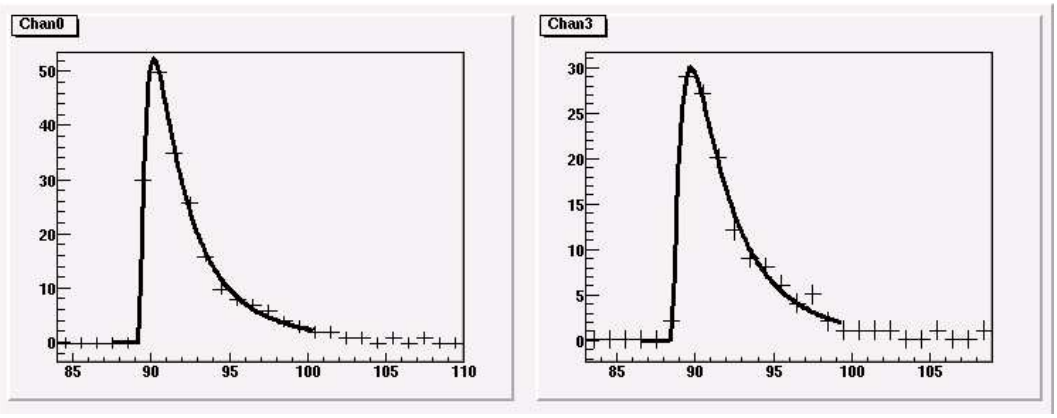

Figure 5.16: Signal Sample with fit superimposed

The time and charge of each signal analyzed is then saved in a text file.

Chapter 6

ULTRA Engineering runs

The ULTRA experiment is currently in a development phase. Two engineering runs were performed, in the Alps region, in order to test and optimize the ETscope and UVscope detectors. In the first engineering run, held in September 2002, the ETscope composed by four stations disposed in a triangle around a central station, was tested. In the second engineering run, held in June 2003, the ETscope composed by five stations disposed in a square around a central station and a first UVscope prototype were tested. The ETscope DAQ system based on the LIP-PAD board was tested and its performance compared with a traditional NIM-CAMAC DAQ system.

6.1 Site Location and Experimental Setup

ULTRA is a hybrid instrument that aims to detect both the electromagnetic component of an EAS and the Čerenkov light produced by its relativistic particles. The experiment site has to satisfy several constrains. The site must have a high altitude in order to maximize the rate of interesting shower events. It must be located far from cities and other light sources in order to minimize the light background. A flat surface large enough to install the ETscope and a nearby hill to install the UVscope are needed. Finally, there are some logistic constrains, such as the accessibility to the site, that must be addressed.

The site selected for these engineering runs was an abandoned quarry in the Alps in the Mont-Cenis region near the French-Italian border. The chosen site was located at the coordinates 45.3° North 6.9° East and had an altitude of 1970m a.s.l. that corresponds to an atmospheric depth of $80\,\mathrm{g\,cm^{-2}}$. The site had an amphitheater shape with a large flat surface in the center. The site was accessible by car and was located near a main road. Yet, the high quarry walls protected the experiment from car lights. Figure 6.1 shows a map of the region, where it is indicated the site location. Figure 6.2 shows a photograph of the experiment site. The photo has been taken from the UVscope location.

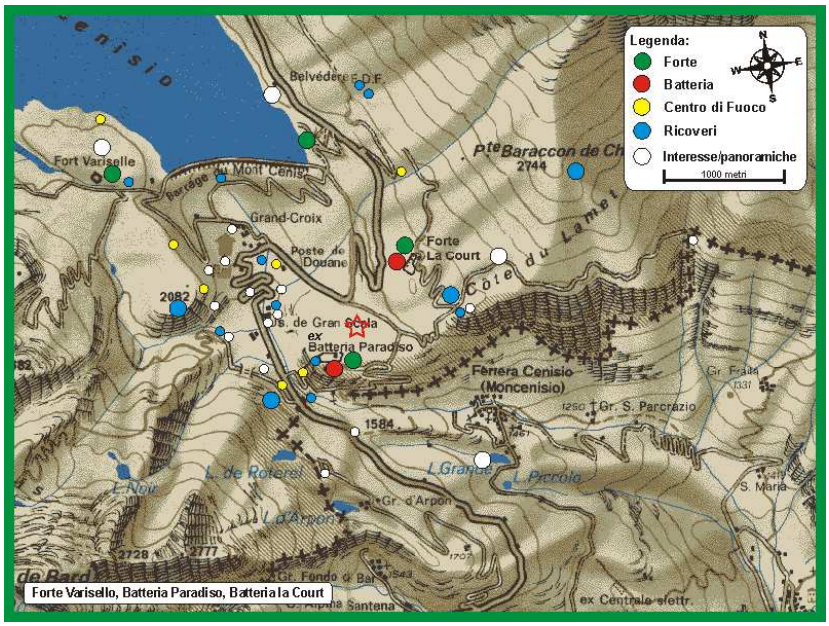

Figure 6.1: ULTRA engineering runs took place in the Alps. The coordinates are 45.3° North 6.9° East. The red star indicates the engineering runs site.

Figure 6.2: Photograph of the experiment site taken from the UVscope location.

The flux of particles at sea level is $\sim 180\,\mathrm{Hz/m^2}$. Each ETscope station has an area of $0.68\,\mathrm{m^2}$. Thus the single particle rate in each station is estimated to be of the order of $\sim 200\,\mathrm{Hz}$.

In the first run the ETscope was placed in the center of the quarry. The ETscope was composed by four stations: three stations were located at the vertexes of a triangle and the fourth at the center of the triangle. Each vertex of the triangle was located 23 m apart from the center.

The geometry of the detectors during the second run is presented in figure 6.3.

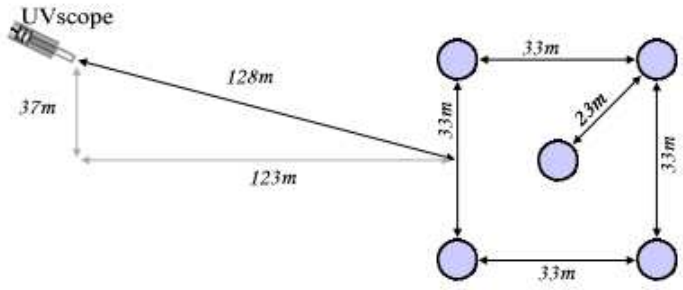

Figure 6.3: The figure depicts the ETscope stations and UVscope arrangement in the second engineering run. The ETscope was installed in a flat surface disposed in a square. Four stations were located in the vertexes of the square and one station was located in the center of the square. The UVscope was placed in a near hill in such a way that its field of view enclosed the area covered by ETscope.

The ETscope was composed by five stations: four stations were disposed in the vertexes of a square and the fifth station was located in the center of the square. The UVscope was placed in the nearby hill pointing downward to the center of the ETscope.

The expected performance of the ETscope can be expressed, as usually done in cosmic ray ground array detectors, as a function of an effective area (A_{eff}). We define A_{eff} for each EAS energy bin as:

$$A_{eff} = \frac{N_{\mathrm{detect}}\,(E)}{\Phi\,(E)\,\Delta E} \cdot \frac{\cos\theta}{\Delta\Omega}$$

where N_{detect} is the number of detected EAS per time unit, $\Phi\,(E)$ is the incident flux of EAS in the energy bin centered at E with an width ΔE, θ is the azimuthal angle and $\Delta\Omega$ is the solid angle covered by the detector.

The A_{eff} is usually estimated using a Monte-Carlo simulation by generating

and throwing to the detector several air showers. In this case A_{eff} is defined as

$$A_{eff} = \frac{N_{\text{detect}}}{N_{\text{throw}}} \cdot A_{\text{throw}} \cos\theta$$

where N_{detect} is the number of events detected, N_{throw} is the number of events generated in a test area (A_{throw}) and θ is the azimuthal angle.

A_{eff} grows with the Energy reaching an asymptotic value (figure 6.4).

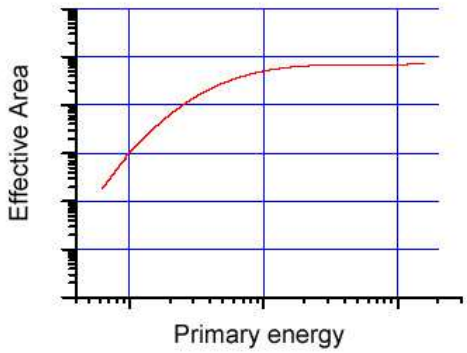

Figure 6.4: Sketch of the effective area for internal events.

The number of events in each Energy bin is then given by

$$n(E)\,\Delta E = A_{eff}(E) \cdot \Phi(E) \cdot \Delta E$$

$\Phi(E)$ is a fast decreasing function of the energy, parametrized by a negative power law

$$\Phi(E)\,dE = I_0 E^{-\gamma} dE$$

The distribution $n(E)\,dE$ has a maximum (figure 6.5) which is usually defined as the energy threshold of the array. The total number of expected events with an energy $E > E_0$ is given by

$$N = I_0 \cdot \Delta T \cdot \Delta\Omega \int_{E_0}^{\infty} E^{-\gamma} A_{eff}(E)\,dE$$

where ΔT is the integration time and $\Delta\Omega$ is the solid angle.

The precise estimation of the ETscope effective area should be performed using a Monte-Carlo simulation. As that was not yet done, a rough estimation was obtained extrapolating the results of EAS-TOP experiment [18, 19]. Table 6.1 summarizes the expected rate for the ETscope as described in [18].

In the engineering runs the signals from each ETscope station was driven, by coaxial cables, to a centralized DAQ. The centralized DAQ was composed by two

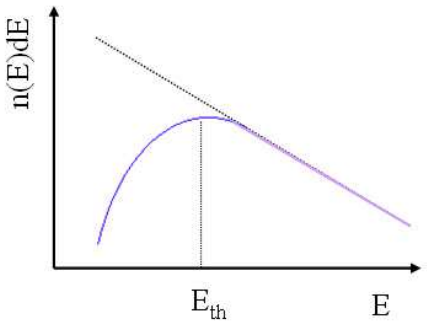

Figure 6.5: Sketch of the number of events detected for a given energy (blue) and of the incident flux (grey). It is also represented the energy threshold of the detector (E_{th}).

Array radius (m)	Atm. depth (g cm^{-2})	Thres. Energy (E_{th}, GeV)	$\Phi\,(E > E_{th})$ (m^{-2}s^{-1}sr^{-1})	$n_{int}\,(E > E_{th})$ (Hz)	(ev./h)
20	810	$2.1 \cdot 10^5$	$1.8 \cdot 10^{-5}$	0.070	252
20	1013	$6.4 \cdot 10^5$	$2.9 \cdot 10^{-6}$	0.012	41
50	810	$7.0 \cdot 10^5$	$2.5 \cdot 10^{-6}$	0.062	224
50	1013	$1.9 \cdot 10^6$	$4.9 \cdot 10^{-7}$	0.012	44

Table 6.1: Expected threshold energy and internal event counting rate of the ETscope array for two different detector separations and two different observation levels.

systems: the NIM-CAMAC system and the LIP-PAD system. The signals from the stations were passively divided and both systems acquired data in parallel. For a description of the NIM-CAMAC system please see [20]. The LIP-PAD system was composed by two LIP-PAD boards controlled by a single PC.

Figure 6.6 represents schematically the DAQ system used in the first run. In

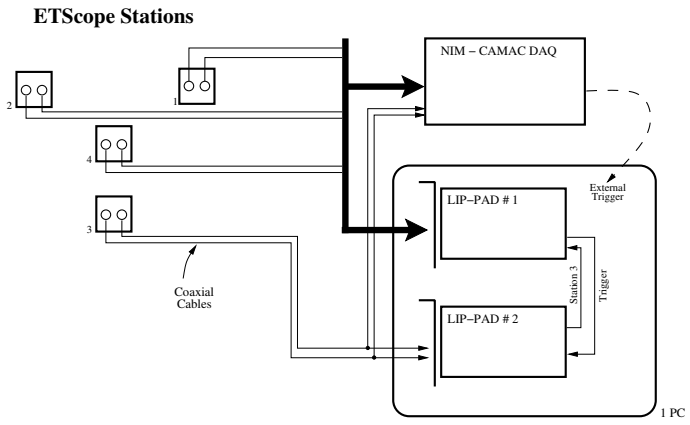

Figure 6.6: ETscope DAQ setup used in the first engineering run

this run the PMTs from the first 3 stations (3×2 PMTs) were connected in one LIP-PAD board (main). The fourth station was connected to the other LIP-PAD board (secondary).

The LIP-PAD boards digitalized the PMTs signals and generated for each station a low level trigger whenever the two PMTs signals of the corresponding station were above a predefined threshold. The trigger signal of the fourth station (generated in the secondary board) was sent online to the main board. The final trigger was generated in the main board combining the stations low level triggers. The final trigger was then sent online to the secondary board so that both boards had the full trigger information. The events data was kept in the internal memory until the boards were read through the PCI bus.

Figure 6.7 represents the DAQ setup used in the second engineering run. In this run, in order to increase the dynamic range, each station, as explained in section 3.1, had a PMT with a low gain (lgPMT) and a PMT with a high gain (hgPMT). The five lgPMT were connected to a LIP-PAD board (slave) while the five hgPMT were connected to the other LIP-PAD board (master). The master board digitalized the hgPMT signals and generated the trigger that was then sent to the slave board. The slave board digitalized the lgPMT signals. With this setup the hgPMT and lgPMT data was acquired using the same trigger based only in the hgPMTs.

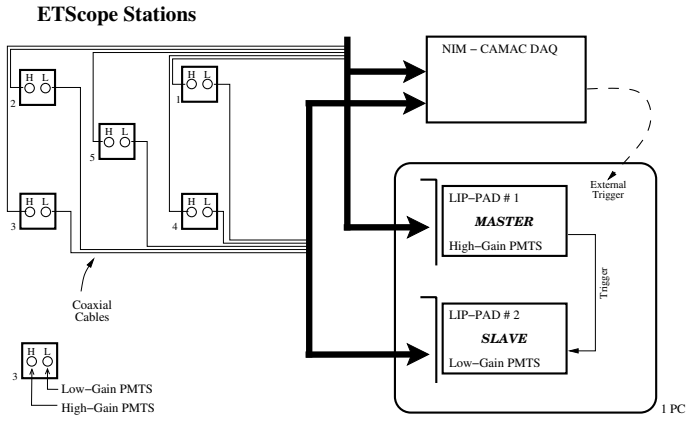

Figure 6.7: Sketch of the effective area for internal events.

6.2 Analysis and experimental results

The LIP-PAD data consists of sets of signal samples taken with a frequency of 100 MHz in a time window of 2.5 μs around the trigger condition. Offline, the signal data is analyzed to extract, for each signal, its charge and start time as explained in chapter 5.5. Using these informations is then possible, after calibration, to perform a global fit event by event reconstructing the energy and the direction of the cosmic ray shower.

The CAMAC data that contains also the information of the charge and time registered in the different stations for each acquired event is used for comparison.

6.2.1 Charge reconstruction

The charge registered in one station is obtained from the LIP-PAD data performing a fit of the expected signal shape to the signal. The performance of the charge reconstruction method (described in section 5.5) is discussed in this section. The results obtained using the LIP-PAD in the first engineering run are presented and compared to those obtained with the CAMAC system.

Figure 6.8 discloses the correlation between the acquired charge from both PMT of the same ETscope station. In each plot the charge acquired from the second PMT of one station is plotted against the one acquired from the first PMT of the same station. The LIP-PAD board data shows a good correlation between the acquired charge from both PMTs of the same station. In fact, due to the geometry of the ETscope stations, described in chapter 3.1, each PMT should receive half of the light signal generated in the scintillator. The CAMAC data does not show such a good correlation. In fact the data is mainly distributed along a straight line but there are many events for which the charge acquired from the second PMT is well below the charge acquired from the first one. This happened

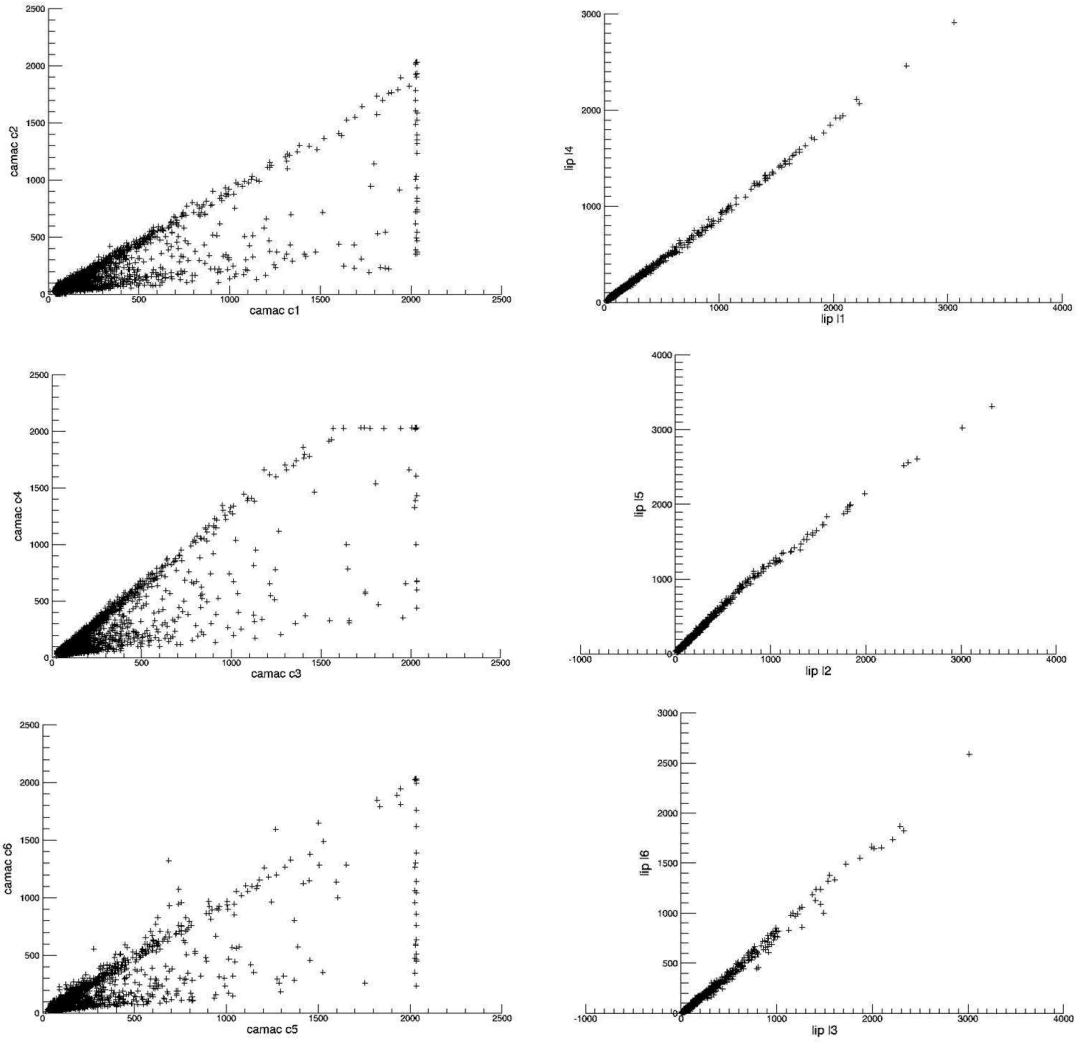

Figure 6.8: Correlation between the acquired charge from both PMT of the same ETscope station in the first engineering run. Left: CAMAC data; right: LIP-PAD data; Top: station 1; middle: station 2; bottom: station 3. In each plot the charge acquired from the second PMT of one station (Y axis) is plotted against the one acquired from the first PMT of the same station (X axis). The CAMAC data is plotted in QDC units while the LIP-PAD data is plotted in ADC units. An acquired event is represented by a cross.

in every station and reflects a problem that occurred in the first engineering run: the CAMAC data acquisition uses a QDC that integrates the signal in a region defined *a priori* from the trigger condition. Each signal must then arrive to the QDC after the trigger has been generated, in the integration window. This is usually done by delaying the signals, driving them through long cables in such a way that the delay in the cable compensate the delay in the trigger generation. During the first engineering run there were problems with the delay of the signals and, sometimes, part of the signals arrived at the QDC outside the integration window, causing the QDC to integrate only a part of the signal, underestimating the charge acquired from the PMT.

Figure 6.9 shows the comparison between the charge reconstructed from the LIP-PAD data and the charge acquired by the CAMAC system for the events with a good (relative deviation $< 10\%$) correlation between the two PMTs. The data presented shows a good correlation between the LIP-PAD data and the CAMAC data. It is then possible to inter-calibrate the LIP-PAD and CAMAC systems.

Figure 6.10 shows that the distributions of LIP-PAD and CAMAC data have the same shape both for single particle data and for data acquired with a shower trigger.

The peak of the spectrum acquired by each PMT in single trigger mode is then used as a conversion factor to estimate, from the integrated charge, the particle density registered in each station for events acquired with the shower trigger.

6.2.2 Time reconstruction

The time reconstruction for each event acquired with the LIP-PAD system relies on a fit to the data samples acquired at 100 MHz as explained in section 5.5. In fact the data taken by the LIP-PAD consists of 256 samples spaced by 10 ns, corresponding to 2.5 μs of data around the trigger condition. As the data is taken synchronously for all the PMTs connected in the same LIP-PAD board the time differences between any two stations can be easily calculated by subtracting the times for the two stations after applying the correction due to different cable lengths and electronics delays. These corrections were measured using the central station as a time reference and placing it successively on the top of each of the other stations.

In the CAMAC system the time of each event is given by a TDC that outputs directly, for each station, the time elapsed from the first signal above a predefined threshold registered for an event.

The time resolution of the detector is, thanks to the geometry used in the second engineering run, easily estimated from the time differences between the several stations. In the second engineering run, 4 ETscope stations were disposed in the vertexes of a square (figure 6.3), which means that there were two sets of parallel sides. The time differences between stations connected by parallel sides

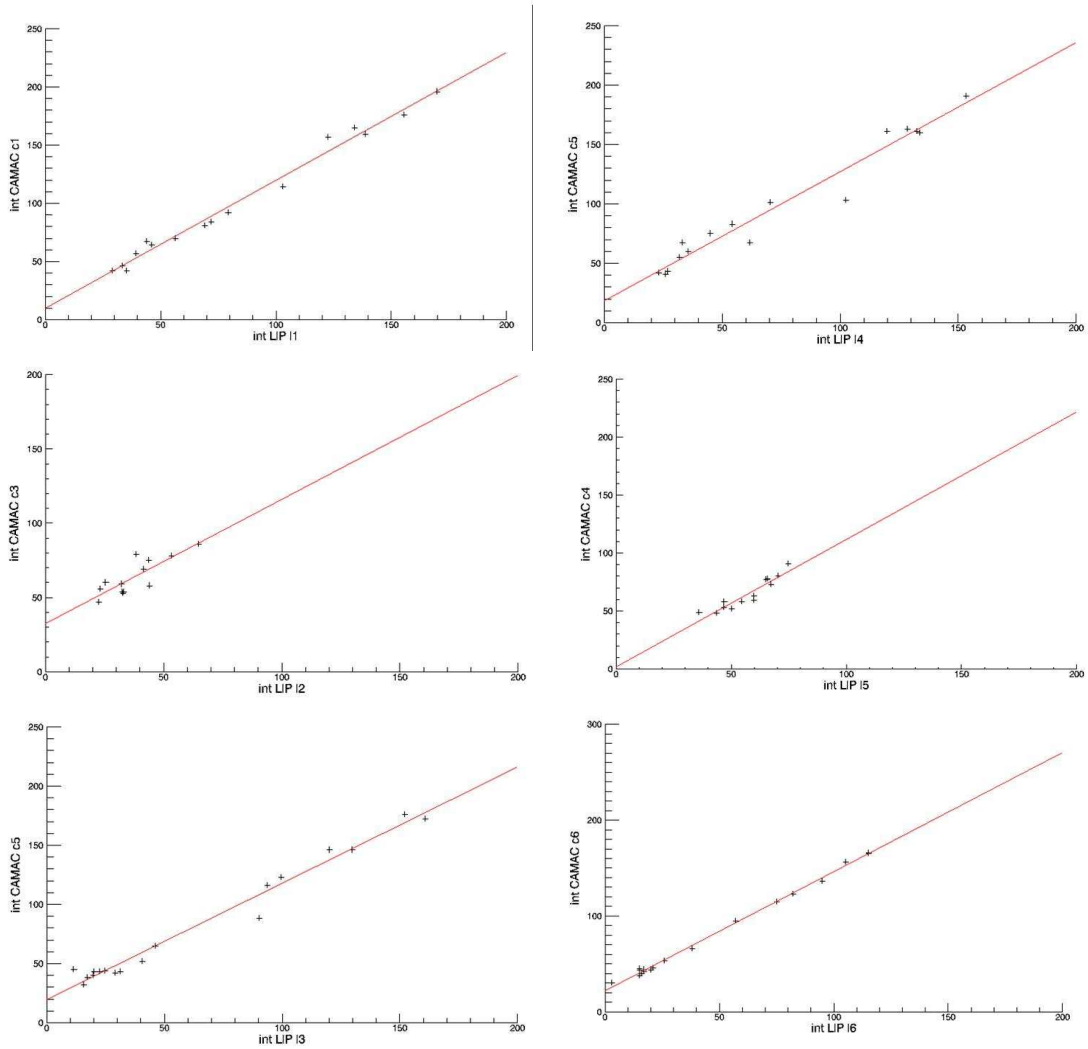

Figure 6.9: Correlation between LIP-PAD and CAMAC data. Top: station 1; middle: station 2; bottom: station 3. The reconstructed charge from the LIP-PAD (X axis) is plotted against the charge acquired with CAMAC (Y axis). The data points and the linear fit are represented by crosses and by a solid line, respectively.

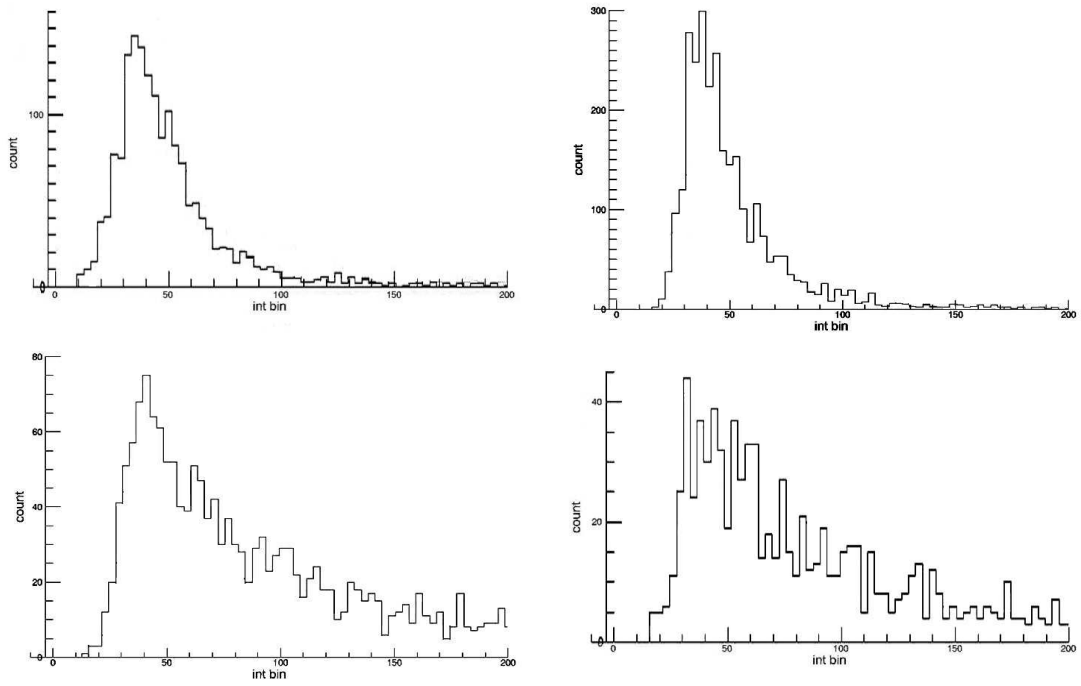

Figure 6.10: Charge distribution of data acquired from the first PMT of station 1. Left: LIP-PAD data; right: CAMAC data; top: single particle trigger; bottom: shower trigger. The LIP-PAD data is plotted in ADC units while the CAMAC data is plotted in QDC units.

should be equal. Thus $t_1 - t_0$ should be equal to $t_2 - t_3$. Then if T_a is defined as

$$T_a = t_1 - t_0 - (t_2 - t_3)$$

its distribution, in the case of an ideal detector, should be a Gaussian with a mean value $\overline{T_a}$ equal to 0 and a dispersion (σ_{T_a}) equal to the shower front width. In a real detector σ_{T_a} reflects the width of the shower front convoluted with the detector time resolution. In the case of the LIP-PAD, data is taken with a sample rate of 100 MHz which introduces an additional 10 ns pattern in the time measurements in each channel (see figure 6.11). This feature introduces a non

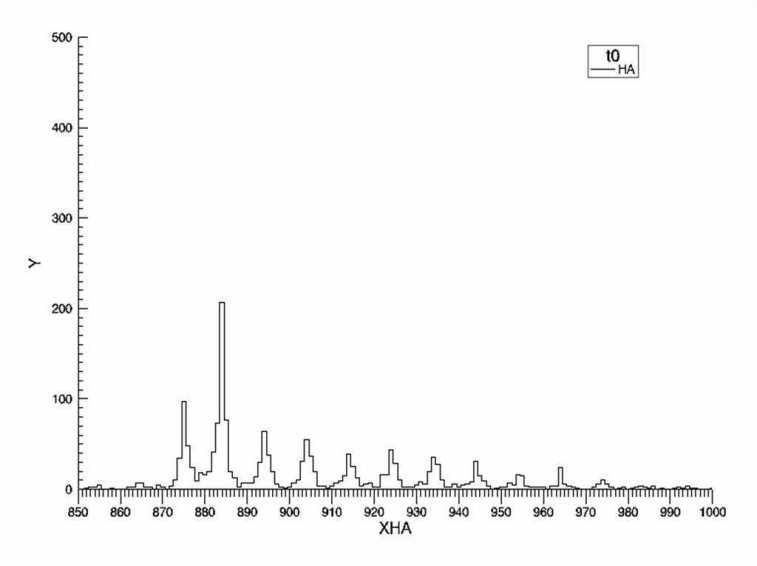

Figure 6.11: Distribution of the event time (T_0) registered in the station 1. The X axis is scaled in ns. The trigger time is set at 1.28 μs.

Gaussian shape in the T_a distribution shown in figure 6.12 .

In figure 6.13 the time resolution of CAMAC and LIP-PAD data is compared. It can be seen from the figure that both data have a similar σ_{T_a} indicating that with both systems the time resolution of the detector can be estimated to be better than 10 ns, in agreement with the requirements expressed in section 3.3.

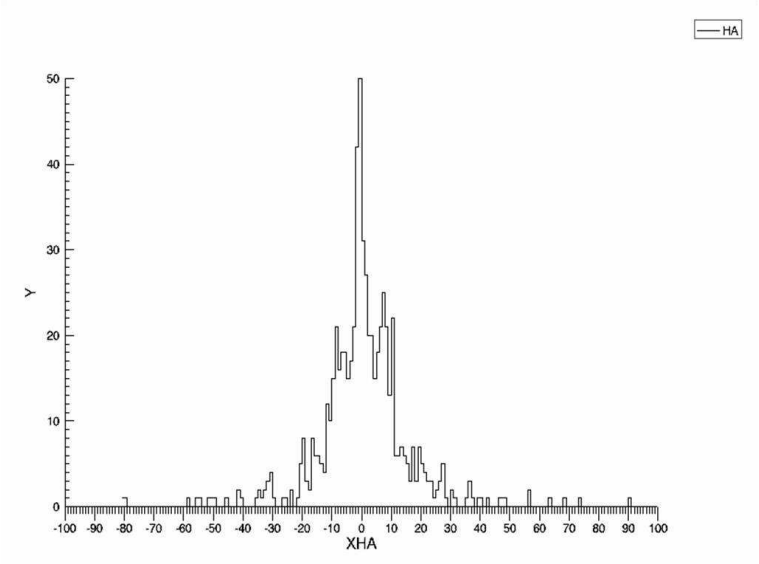

Figure 6.12: Distribution of T_a variable defined in the text. The X axis represents time in ns.

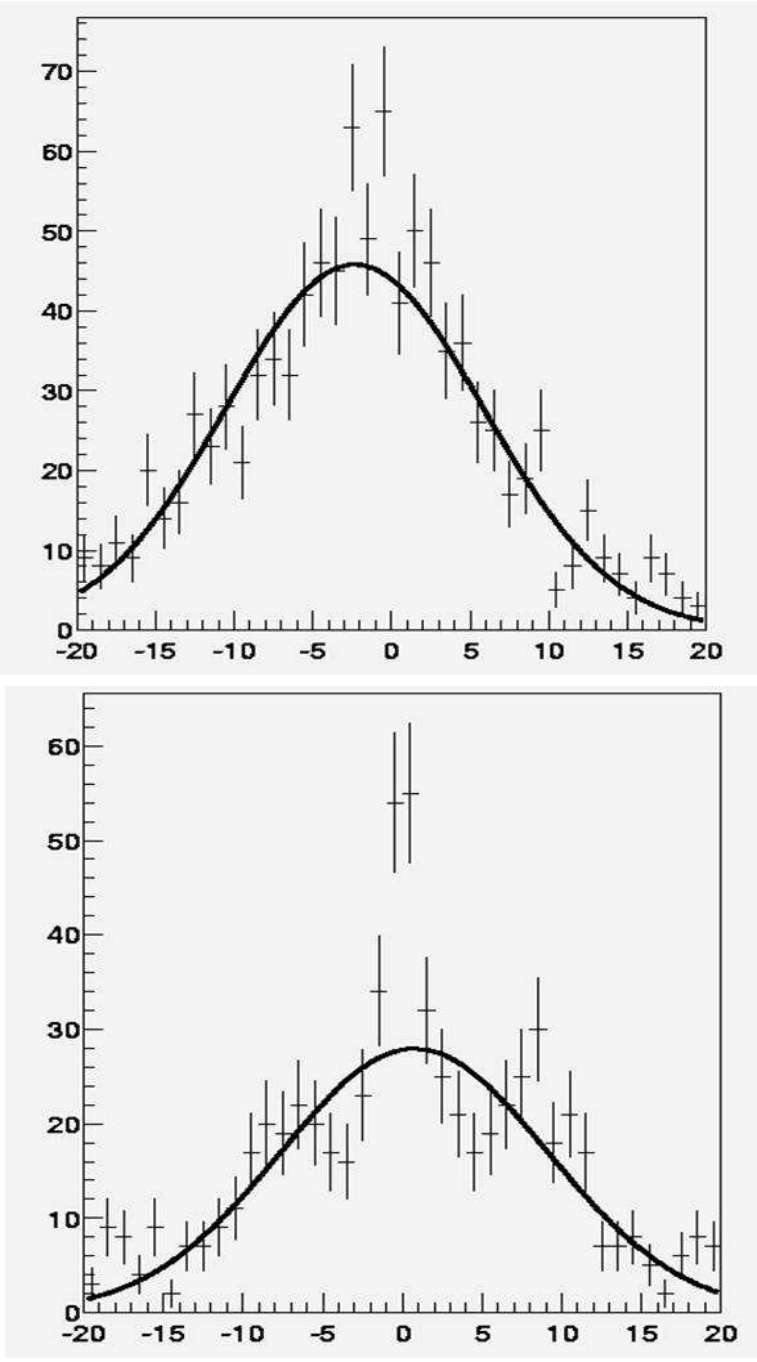

Figure 6.13: Time resolution distribution. Top: CAMAC data; bottom: LIP-PAD data. The X axis represent time in ns.

6.2.3 Shower reconstruction

The shower parameters, i.e., its arrival direction, core position and size, can be estimated from the particle density registered in each station and the time differences between them. For this purpose the LIP group has developed, using ROOT and C++, an integrated simulation and analysis package taking into account the full detector geometry. In the simulation, the showers are generated and the charge and time in each station are predicted. In the analysis the algorithm described below is implemented.

The arrival direction of the shower is computed by triangulation using the time of flight technique [21].

Assuming a planar shower front moving at c and neglecting possible altitude differences between the stations, the impact time t_{o_i} at station i with coordinates (x_i, y_i) is written as

$$t_{0_i} = T_0 - \frac{\sin\theta\cos\varphi \cdot x_i + \sin\theta\sin\varphi \cdot y_i}{c}$$

Using three non collinear stations, three independent equations can be written to determine T_0, θ, φ. The errors due to the time resolution of the stations are minimized in the second engineering array, which has four stations placed in the vertexes of a square (0, 1, 2 and 3 in figure 6.14), using average time differences between the detectors placed in parallel sides. In fact the time differences computed for each pair of parallel sides should be equal. It is then possible to define a virtual setup with three stations (A, B and C in figure 6.14) in which the time

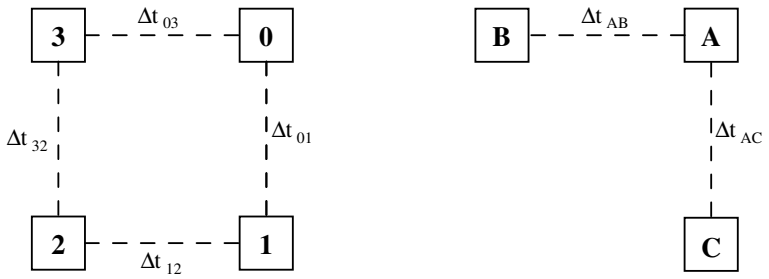

Figure 6.14: Left: real array; right: virtual array

difference for each side are computed from the measured values. Taking into account that it is expected that the shower front arrival time estimation is more accurate in stations detecting higher particle density, the mean time differences values are computed from:

$$\Delta t_{AB} = \frac{(\rho_1 + \rho_2)\,\Delta t_{12} + (\rho_3 + \rho_0)\,\Delta t_{03}}{\rho_0 + \rho_1 + \rho_2 + \rho_3}$$

$$\Delta t_{AC} = \frac{(\rho_0 + \rho_1)\,\Delta t_{01} + (\rho_2 + \rho_3)\,\Delta t_{32}}{\rho_0 + \rho_1 + \rho_2 + \rho_3}$$

where ρ_0, ρ_1, ρ_2 and ρ_3 stands for the particle density detected in each station.

The distance between the stations that is an input to the algorithm has been corrected performing a simple mean:

$$\Delta x, y_{AC} = \frac{\Delta x, y_{01} + \Delta x, y_{32}}{2}$$

$$\Delta x, y_{AB} = \frac{\Delta x, y_{03} + \Delta x, y_{12}}{2}$$

The azimuthal angle φ is computed as:

$$\tan\varphi = \frac{\Delta t_{AC}\Delta x_{AB} - \Delta t_{AB}\Delta x_{AC}}{-\Delta t_{AC}\Delta y_{AB} - \Delta t_{AB}\Delta y_{AC}}$$

The zenithal angle can be calculated using the side AB or AC:

$$\sin\theta_{AB,AC} = \frac{c \cdot \Delta t_{AB,AC}}{\Delta x_{AB,AC}\cos\varphi + \Delta y_{AB,AC}\sin\varphi}$$

The zenithal angle will be taken as the mean value taking into account the fact that the greater the time differences, the greater the accuracy of the result:

$$\sin\theta = \frac{\Delta t_{AB}\sin\theta_{AB} + \Delta t_{AC}\sin\theta_{AC}}{\Delta t_{AB} + \Delta t_{AC}}$$

The shower core can be evaluated using simple methods. The first one is the barycenter method in which the shower core coordinates (x_c, y_c) are given by

$$x_c = \frac{\sum_i \rho_i x_i}{\sum_i \rho_i}$$

$$y_c = \frac{\sum_i \rho_i y_i}{\sum_i \rho_i}$$

A more precise method is the circle algorithm [22, 23]. The method consists in writing, for each station k the equation of a circumference with the center in the station (x_k, y_k) and the radius (r_k) equal to the distance of the station to the shower core:

$$(x_c - x_k)^2 + (y_c - y_k)^2 = r_k^2 \quad k = 1, 2, 3$$

each circumference then contains the shower core point (x_c, y_c) and the intersection of three of them gives an unique solution for the shower core location. The distance of a station to the shower core can be estimated, if the shower size is known, from the particle density registered in the stations. Using a simplified version of the NKG LDF the particle density in station k (ρ_k) can be related to the density in the first station (ρ_1) as:

$$\frac{\rho_k}{\rho_1} = \left(\frac{r_1}{r_k}\right)^{\alpha'} \quad k = 2, 3$$

where r_k is the distance from station k to the shower core point, r_1 is the distance of the shower core from station 1 and α' is an effective parameter, adjusted to approximate the NKG behaviour as much as possible. It is then possible to write r_k as a function of r_1

$$r_k = \left(\frac{\rho_1}{\rho_k}\right)^{\frac{1}{\alpha'}} \cdot r_1 \quad k = 2, 3$$

Solving the system of five equations the shower core location is obtained. If the circle algorithm doesn't converge the core is estimated by the barycenter method.

Finally, the size of the shower (N_e) can be estimated from an iterative fit of the registered particle densities in each station to the lateral profile of the shower given by the NKG formula.

$$\rho(r) = c(s)\,\frac{N_e}{r_0^2}\left(\frac{r}{r_0}\right)^{s-2}\left(1 + \frac{r}{r_0}\right)^{s-4,5}$$

where

$$c(s) = 0,366 \cdot s^2 \cdot (2,07 - s)^{1,25}$$

The shower age (s) is computed as:

$$s = \frac{3t}{t + 2\beta}$$

and t, the atmosphere traversed by the shower, is calculated as:

$$t = \frac{\mathrm{p}}{\cos\theta \cdot \mathrm{r.l.}}$$

where p is the atmospheric depth, λ is the radiation length in the air and θ is the shower zenithal angle.

For the fit the initial value for the shower energy is taken as $E_i = 1\,\mathrm{PeV}$. The parameter β_i is estimated by

$$\beta_i = \ln\left(\frac{E_i}{E_c}\right)$$

being $E_c = 81\,\mathrm{MeV}$, the electron critical energy.

From β_i one can obtain the estimation for the initial value of the shower size (N_e) from the following equations. The longitudinal profile parametrization (see section 2.1) can be written as

$$e^{\alpha'_i} = (t + 2\beta_i) \cdot \beta_i^{-\frac{1}{3t}}$$

where

$$\alpha'_i = \frac{3t\ln(3t) - \alpha_i}{3t}$$

and

$$\alpha_i = -2\left(\ln(N_{e_i}) - \ln(0.31) - t\right)$$

Usually, the fit converges quickly and after a few iterations a good estimation of N_e and of the shower core location are obtained.

In figure 6.15 the distribution of the arrival direction (zenith and azimuthal angles) for shower events is plotted for events acquired with the LIP-PAD system and the CAMAC system.

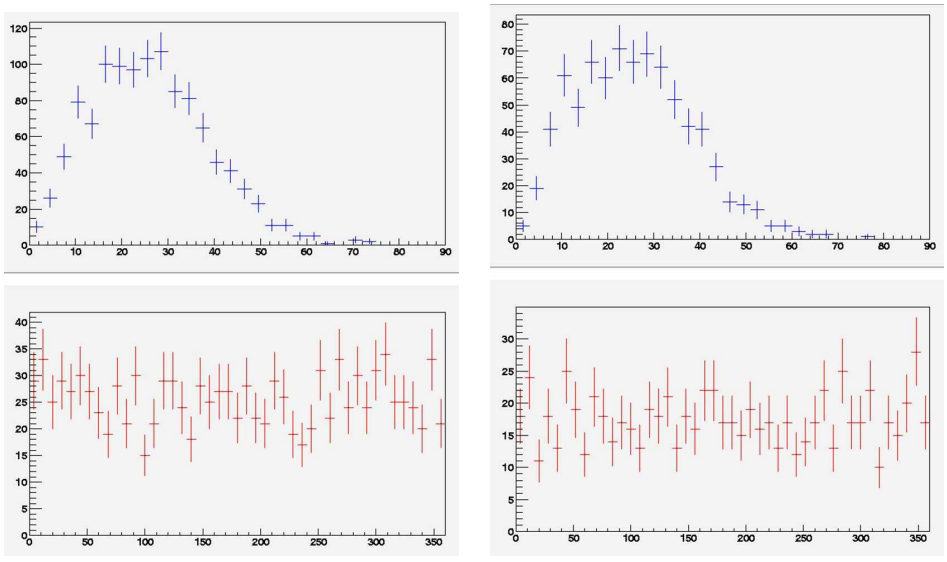

Figure 6.15: Distribution of the arrival direction for shower events. Left: CAMAC data; right: LIP-PAD data; top: distribution of the zenith angle (θ) in degrees; bottom: distribution of the azimuthal angle (φ) in degrees.

Figure 6.16 represents the distribution of the reconstructed shower size (N_e) for data acquired with LIP-PAD and CAMAC systems.

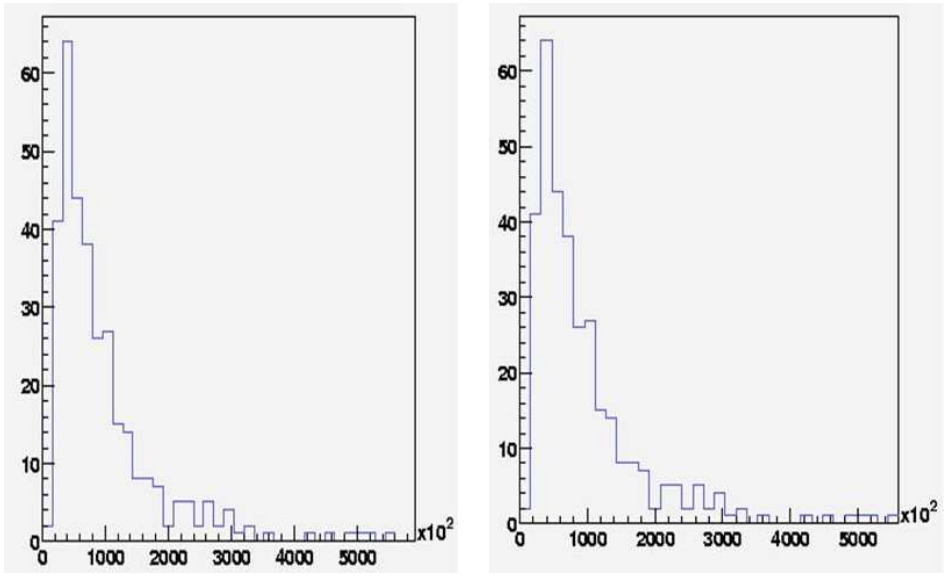

Figure 6.16: Distribution of the reconstructed shower size (N_e). Left: CAMAC data; right: LIP-PAD data.

The results show a good agreement between the data acquired by the two systems.

Chapter 7

Summary and Perspectives

The ULTRA experiment aims to provide quantitative measurements of the UV light produced, and reflected in the Earth surface, by an EAS traversing the atmosphere. The main concept of ULTRA is to use an UV optical detector to collect the UV light generated by an EAS which is simultaneously detected with a conventional ground array of scintillators.

The DAQ system of ULTRA must acquire, upon a trigger condition, the several PMT signals from which the particle density in each station and the time between the registered signals are estimated. In the option of a distributed DAQ system, where each station runs in an autonomous way, each acquired signal must be time-tagged in relation to a time reference common to all units and the time differences between the several stations are computed offline. The time differences between the acquired signals are used to compute the shower direction and must be estimated with a precision better than 10 ns to meet the requirement of a precision of 8° in the estimation of the shower direction. The shower size and core point are estimated from the particle density at each station and the shower direction.

The ability to use a low cost, commercially available, GPS to synchronize a wireless, stand-alone, custom designed data acquisition board and detectors was studied. The data acquisition system of ULTRA was thus designed using the GPS system to provide the synchronization pulse at each second. The GPS is operated in differential mode for improved accuracy. The differential accuracy of the PPS pulses between two co-located UT+ GPS receivers was studied. The distribution of the time differences between the synchronization pulses from the two GPS receivers had a Gaussian shape with a mean value of 8.3 ns and a dispersion of 2.2 ns that reflect the precision of the synchronization pulses and is well below the required precision of 10 ns.

A specific board, the LIP-PAD board, was developed in cooperation with the Lisbon Cosmic Ray Telescope (TRC), to be the core of the ULTRA DAQ system. The LIP-PAD board is a PCI based board with six analog acquisition channels, each having a 100 MHz, 10 bits, flash ADC, that can measure, using an oscillator

and a counter coupled to a TDC, time intervals with a dynamic range wider than 1 s and a resolution of few nanoseconds. The LIP-PAD synchronized by the PPS pulse generated by the GPS is able to time-tag any event with an accuracy better than 10 ns.

The ULTRA experiment is currently in a development phase. Two engineering runs were performed in September 2002 and June 2003, in the Alps region, in order to test and optimize the ETscope and UVscope detectors. In the engineering runs of ULTRA the LIP-PAD has been tested with the ETscope and its performance compared to a traditional NIM-CAMAC DAQ system. As an outcome of these tests the LIP-PAD has been chosen as the DAQ system of the ULTRA experiment, since it is a compact system that can integrate a distributed wireless DAQ system, having the capability of time-tagging events and has a performance greater than the traditional system.

More recently the ULTRA apparatus has been mounted in the soccer camp of LPSC laboratory in Grenoble to be possible to test, understand and solve the problems with the development of the final version of UVscope detector. Currently, a stereoscopic version of the UVscope detector has been mounted, using the LIP-PAD DAQ system, and, although in background rich environment, there are already encouraging results.

The ULTRA experiment is now ready for physics runs that are expected to take place in the spring 2005 in Sicily.

Bibliography

[1] B. Rossi, "Raggi Cosmici," 1971.

[2] L. Scarsi, "The extreme universe of cosmic rays: Observations from space," *NUOVO CIMENTO*, vol. C24, p. 471, 2001.

[3] M.A. Lawrence, R.J.O. Reid and A.A. Watson, "The cosmic ray energy spectrum above 4×10^{17} eV as measured by the Haverah Park array," *J. Phys. G: Nucl. Part. Phys.*, vol. 17, pp. 733–757, 1991. and references therein.

[4] K. Greisen *Progr. in Cosmic Ray Physics*, vol. 3, p. 1, 1956.

[5] K. Kamata *et al. Prog. Theor. Phys. suppl.*, vol. 6, p. 93, 1958.

[6] N. Chiba *et al.*, "Akeno Giant Air Shower Array (AGASA) covering $100\,\mathrm{km}^2$ area," *Nucl. Instr. Methods*, vol. A311, pp. 338–349, 1992.

[7] J. N. Matthews, "Description of the High Resolution Fly's Eye detector," in *Proceedings of* 27^{th}*ICRC*, p. 350, 2001.

[8] J. Bluemer, "Status And Perspectives Of The Pierre Auger Observatory," in *Proceedings of the* 28^{th}.

[9] C. Baixeras, "The MAGIC Telescope," *Nucl.Phys.B (Proc.Suppl.)*, vol. 114, pp. 247–252, 2003.

[10] M.C. Espirito-Santo, P. Goncalves, M. Pimenta, "Applications of GEANT4 in Astroparticle Experiments," *IEEE Transactions on Nuclear Science*, vol. 51, no. 4, p. 1373, 2004.

[11] S. Agostinelli, J. Allison, K. Amako, "GEANT4 - a simulation toolkit," *NIM*, vol. A506, pp. 250–303, 2003.

[12] M.C. Espirito-Santo *et al.*, "Final Report on Radiation Interaction Simulations for High Energy Astrophysics experiments EUSO and AMS," internal note, ESA, 2004.

[13] Motorola, *Oncore Users Guide*, 1998. Can be found at http://www.motorola.com/ies/GPS/pdfs/trm003.zip.

[14] ACAM, *TDC-GP1 Functional Description*, 2001. Can be found at http://www.acam.de/documents/DB_GP1_e.PDF.

[15] ACAM, *ATMD Manual*, 2000. Can be found at http://www.acam.de/documents/DB_ATMD_e.PDF.

[16] P. Silva, "Simulação de cascatas de partículas na atmosfera e sua interacção com o Telescópio de Raios Cósmicos," internal report, LIP-TRC.

[17] G. Knoll, *Radiation Detection and Measurement*. 2 ed.

[18] O. Catalano *et al.*, "ULTRA Technical Report," *EUSO-SEA-REP-001-1*, 2002.

[19] M. Aglietta *et al.*, "The EAS-TOP Array at $E_0 = 10^{14} - 10^{16}$ eV : Stability and Resolutions," *Nucl. Instr. Methods*, vol. A277, pp. 23–28, 1989.

[20] P. Vallania *et al.*, "The ETscope Ground Array for the ULTRA Experiment," in *Proceedings of the* 28^{th} *ICRC*, p. 1053, 2003.

[21] P. Billoir, "Reconstruction of showers with the ground array: status of the prototype array," gap-2000-025, Auger Collaboration, 2000.

[22] O. Catalano internal report, IFCAI-Palermo, 1997.

[23] M.C. Espirito-Santo private comunication.

Appendix A

Acronyms

AAS	-	Analog Acquisition Subsystem
ACAM	-	Electronics manufacturer
ADC	-	Analog to Digital Converter
AGASA	-	Akeno Giant Air Shower Array
ALTERA	-	Altera Corporation - electronics manufacturer
a.s.l.	-	above sea level
ATMD	-	Acam Time Measuring Device
Belenos	-	UV photon detector for direct Čerenkov detection
C	-	Programming language - Successor of B (which is the successor of BCPL = Basic Combined Programming Language)
C++	-	Programing language - Successor of C (++ is the C increment operator)
CAMAC	-	Computer Automated Measurement And Control
CERN	-	European Organization for Nuclear Research
CNR	-	Consiglio Nazionale delle Ricerche, Italy
DAQ	-	Data Acquisition
DTU	-	Digital Trigger Unit
EAS	-	Extensive Air Shower
EASTOP	-	extensive air shower detector installed at Campo Imperatore - almost on top of Laboratori Nazionali del Gran Sasso, Italy
ETscope	-	EAS Telescope
EUSO	-	Extreme Universe Space Observatory
FIFO	-	First In - First Out
Geant4	-	A toolkit for simulation of the passage of particles through matter
GP1	-	TDC chip from ACAM
GPS	-	Global Positioning System

GUI	-	Graphical User Interface
hgPMT	-	high gain PMT
HiRes	-	High Resolution Fly's Eye Cosmic Ray Observatory
HV	-	High Voltage
IASF	-	Istituto di Astrofisica Spaziale e Fisica Cosmica - CNR, Italy
IASF-Palermo	-	IASF-CNR at Palermo, Italy (formerly IFCAI)
ISS	-	International Space Station
LABVIEW	-	Programming language from National Instruments
LASER	-	Light Amplification by Stimulated Emission of Radiation
LDF	-	Lateral Distribution Function
lgPMT	-	low gain PMT
Linux	-	Open source operating system
LIP	-	Laboratório de Instrumentação e Física Experimental de Partículas, Portugal
LIP-PAD	-	LIP- Placa de Aquisição de Dados
LPSC	-	Laboratoire de Physique Subatomique et de Cosmologie, Grenoble, France
LSB	-	Least Significant Byte
LV	-	LabView
MAGIC	-	Major Atmospheric Gamma-ray Imaging Čerenkov
MIP	-	Minimum Ionizing Particle
Motorola	-	Electronics manufacturer
MSB	-	Most Significant Byte
MSPS	-	Mega Samples Per Second
National Semiconductor	-	Electronics Manufacturer
NIM	-	Nuclear Instrumentation Modules
NKG	-	Nishimura-Kamata-Greisen
OpAmp	-	Operational Amplifier
PAO	-	Pierre Auger Observatory
PC	-	Personal Computer
PCI	-	Peripheral Component Interconnect (or Interface)
PCIProbe	-	Software developed at CERN to test PCI peripherals
PLD	-	Programmable Logic Device
PMT	-	Photo Multiplier Tube
ppm	-	parts per million
PPS	-	Pulse Per Second
PVC	-	Poly(Vinyl Chloride) plastic
QDC	-	charge to Digital Converter
RAM	-	Random Access Memory

RC filter	-	Electronics filter composed by a Resistor and a Capacitor
ROOT	-	An Object-Oriented Data Analysis Framework developed at CERN
RS-232	-	A serial communication standard protocol
SNR	-	Signal-to-Noise Ratio
TDC	-	Time to Digital Converter
TDC-GP1	-	Transistor-Transistor Logic
TMS	-	Time Measuring Subsystem
TRC	-	Telescópio de Raios Cósmicos
TTL	-	Transistor-Transistor Logic
UHECR	-	Ultra High Energy Cosmic Rays
ULTRA	-	UV Light Transmission and Reflection in Atmosphere
UT+	-	GPS model from Motorola
UTC	-	Coordinated Universal Time
UV	-	Ultra Violet
UVscope	-	UV Telescope